AD-A065 986 WASHINGTON UNIV ST LOUIS MO LAB FOR APPLIED ELECTRON--ETC F/G 17/2
GAAS ELECTROABSORPTION AVALANCHE PHOTODIODE WAVEGUIDE DETECTORS--ETC(U)
DEC 76 C M WOLFE, W S CHANG, R O GREGORY N00014-75-C-1155

UNCLASSIFIED NL

| OF |
ADA
065986

END
DATE FILMED
5-79
DDC

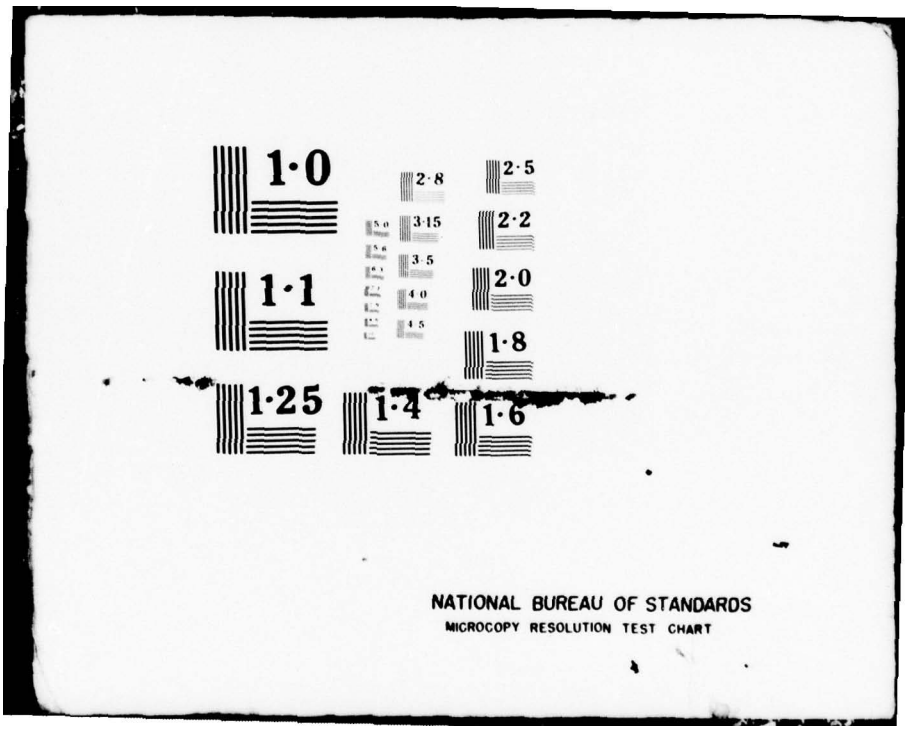
1·0
1·1
1·25
1·4
1·6
1·8
2·0
2·2
2·5
2·8
3·15
3·5
4·0
4·5
5·0
5·6
NATIONAL BUREAU OF STANDARDS
MICROCOPY RESOLUTION TEST CHART

(6)

GaAs ELECTROABSORPTION AVALANCHE PHOTODIODE WAVEGUIDE DETECTORS.

(10)

by

C.M. Wolfe, W.S.C. Chang, R.O. Gregory
M.J. Sun and K.H. Nichols
Laboratory for Applied Electronic Sciences
Washington University
St. Louis, Missouri 63130

(9) Final Report,
(11) December, 1976

(12) 66p.

(15) Prepared Under Contract No. N00014-75-C-1155
for

Dr. David Lewis
Code 221
Office of Naval Research
Arlington, Virginia 22217

GaAs ELECTROABSORPTION AVALANCHE PHOTODIODE WAVEGUIDE DETECTORS

1. INTRODUCTION

There has been substantial recent interest in optical information transfer and processing systems because of their present and potential advantages over conventional electronic systems. These advantages include elimination of interference and ground-loop problems; achievement of wide bandwidths and increased security; and reductions in weight, size, and cost. To achieve these advantages, the realization of GaAs-based integrated optical circuits (IOCs) appears to be particularly promising since coherent light sources, optical detectors, modulators, and other active devices can potentially be integrated on the same substrate with passive devices.

For wide bandwidth IOCs a critical component is the optical detector which must have internal gain to provide optimum sensitivity.[1] This internal gain can be obtained in photovoltaic detectors by means of avalanche multiplication and wide-bandwidth, high-gain, low-noise avalanche photodiodes have been fabricated in GaAs.[2] However, the response of these conventional GaAs avalanche photodiodes decreases rapidly for wavelengths longer than about 0.86μm, and these detectors are not very suitable for the detection of room temperature GaAs and low-Al content AlGaAs laser emision. This is because the detector response depends on band-to-band absorption, whereas the laser emission usually involves band-to-acceptor transitions. Thus, the GaAs laser emission occurs at an energy below the usual long-wavelength cutoff of a GaAs avalanche photodiode.

Recently, however, a new mode of operation has been obtained [3] for these detectors in which absorption below the usual GaAs band edge is enhanced by an electric field (electroabsorption). Compared to the conventional GaAs avalanche photodiode, these GaAs electroabsorption avalanche photodiode (EAP) detectors have their maximum response at wavelengths beyond the normal absorption edge of GaAs. It is this feature that makes the GaAs EAP detectors particularly attractive for GaAs-based IOCs. That is, they can be used to detect the below band edge radiation from GaAs lasers which is transmitted through GaAs waveguide structures with low-loss.

In this report we analyze the properties of these GaAs EAP detectors in GaAs waveguides, describe the fabrication processes, and measure their properties at laser wavelengths of 0.905, 0.915, and 1.06μm. The suitability of these detectors for processing analogue and digital optical signals is then evaluated, and methods for utilizing them in time- and frequency-demultiplexing receiver subsystems are described.

2. ANALYSIS

The configuration used to analyze the waveguide Schottky barrier EAP detector is shown in Fig. 1. The active region of the device which guides and absorbs radiation is doped at a level N cm^{-3} while the substrate is doped at N_s cm^{-3}. To obtain guiding in the active region, N_s must be much greater than N. A reverse-bias voltage -V is applied to the device

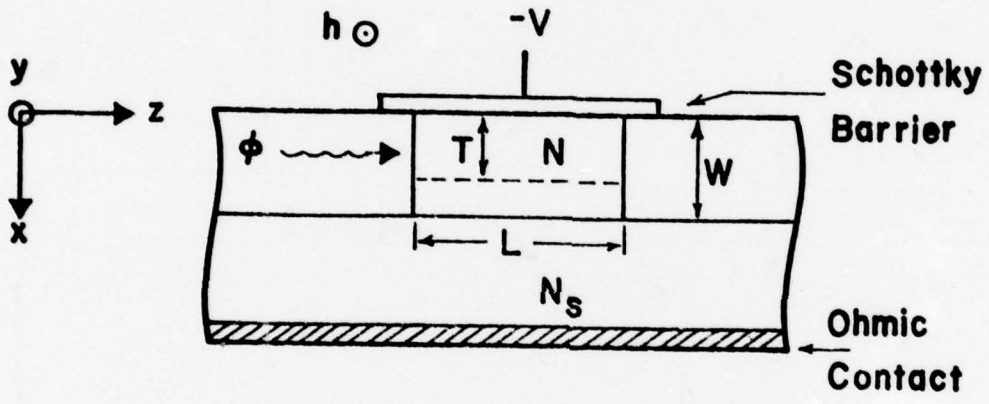

Fig. 1 Schematic of GaAs EAP waveguide detector.

between the Schottky barrier and the ohmic contact. Assuming a uniform doping level N, the space charge in the depletion region under the Schottky barrier is uniform with width T.

2.1 Electric Field Distribution

The electric field distribution in the depletion layer can be determined from Poisson's equation. We first consider the case where the width of the depletion region T is less than the thickness of the guiding layer W. Under this condition the electric field is given by

$$E(X) = \frac{qN}{\varepsilon}X - \frac{2V}{T} \qquad (2\text{-}1)$$

where $T = \left(\frac{2\varepsilon V}{qN}\right)^{\frac{1}{2}}$ and X is the distance from the Schottky barrier.

The second case is when $T \geq W$. Since to obtain guiding in the active layer $N_s >> N$, the space charge region can be approximated by $T \simeq W$, $E(W) \neq 0$. The solution of Poisson equation for the electric field is

$$E(X) = \frac{qN}{\varepsilon}X + E(0), \qquad (2\text{-}2)$$

and the reverse bias voltage is

$$V = -\int_0^W E(X)\,dX = -WE(0) - \frac{qN}{2\varepsilon}W^2. \qquad (2\text{-}3)$$

The pinch-through bias voltage V_p is the bias such that $E(W) = 0$, so

$$V_p = \tfrac{1}{2}E(0)\cdot W = qNW^2/2\varepsilon.$$

From Equation (2-3), we obtain

$$V = -WE(0) - V_p.$$

Therefore,

$$E(0) = -(V + V_p)/W,$$

and

$$E(W) = -(V - V_p)/W,$$

where $V \geq V_p$. The field distribution can be written as

$$E(X) = qNX/\varepsilon - (V + V_p)/W. \qquad (2\text{-}4)$$

2.2 Avalanche Breakdown

When the applied reverse bias is sufficiently large, electrons and holes in the depletion region gain enough energy to produce electron-hole pairs by collisions. The ionization coefficient is defined as the number of electron-hole pairs ionized by a single carrier in a unit distance. The electron and hole current densities at a given bias voltage can be obtained from the continuity equations,

$$\frac{dJ_n(X)}{dX} = \alpha_n(X)J_n(X) + \beta_p(X)J_p(X), \qquad (2\text{-}5)$$

$$\frac{dJ_p(X)}{dX} = -\alpha_n(X)J_n(X) - \beta_p(X)J_p(X), \qquad (2\text{-}6)$$

where J_n and J_p are the current densities of electrons and holes, respectively, α_n and β_p are the ionization coefficients of electrons and holes respectively, and $J_n(X) + J_p(X) = J =$ constant. From Eq. (2-5), we can obtain an expression for the

total current density as

$$J = \frac{J_n(0) + J_p(W)e^{-\int_0^W (\alpha_n - \beta_p)dX}}{e^{-\int_0^W (\alpha_n - \beta_p)dX} - \int_0^W \beta_p e^{-\int_0^X (\alpha_n - \beta_p)dX'} dX}. \quad (2\text{-}7)$$

From Eq. (2-6), we obtain

$$J = \frac{J_n(0) + J_p(W)e^{-\int_0^W (\alpha_n - \beta_p)dX}}{1 - \int_0^W \alpha_n e^{-\int_0^X (\alpha_n - \beta_p)dX'} dX}. \quad (2\text{-}8)$$

Equations (2-7) and (2-8) are equivalent, and the avalanche breakdown voltage can be determined from the condition

$$\int_0^W \beta_p e^{\int_X^W (\alpha_n - \beta_p)dX'} dX = 1,$$

or

$$\int_0^W \alpha_n e^{-\int_0^X (\alpha_n - \beta_p)dX'} dX = 1,$$

since the ionization coefficients α_n and β_p are strongly dependent upon the electric field. This dependence of α_n and β_p on field has been determined experimentally by measuring the breakdown voltages for different device doping levels.[4]

With this data the break down voltages of GaAs Schottky-barrier diodes were calculated as a function of layer thickness for various doping levels as shown in Fig. 2. Also shown in the lower part of the figure is the maximum electric field at breakdown as a function of thickness for various doping levels. The ionization coefficients used[5] in these calculations were

$$\alpha_n = 2 \times 10^6 \exp(-2 \times 10^6/E),$$

and

$$\beta_p = 10^5 \exp(-5 \times 10^5/E).$$

Eqs. (2-1) and (2-4) were used to determine the dependence of the electric field on X.

2.3 Electroabsorption

The absorption of photons with energy less than the energy gap of the device is expected to increase in the presence of an electric field.[6] This Franz-Keldysh electroabsorption coefficient for GaAs is given by

$$\alpha(W,E) = \frac{10^4}{n} E^{1/3} \sum_j \left(1 + \frac{M}{M_{v_j}}\right)\left(\frac{2\mu_j}{M}\right)^{4/3} \times \left[(A_i'(\beta_j))^2 - \beta_j A_i^2(\beta_j)\right], \qquad (2\text{-}9)$$

where

$$\beta_j = 1.1 \times 10^5 (Eg - \hbar\omega)\left(\frac{2\mu_j}{M}\right)^{1/3} E^{-2/3}$$

A_i is the Airy function, n is the refractive index, Eg is the energy gap, $\hbar\omega$ is photon energy, Mv_j are the effective masses

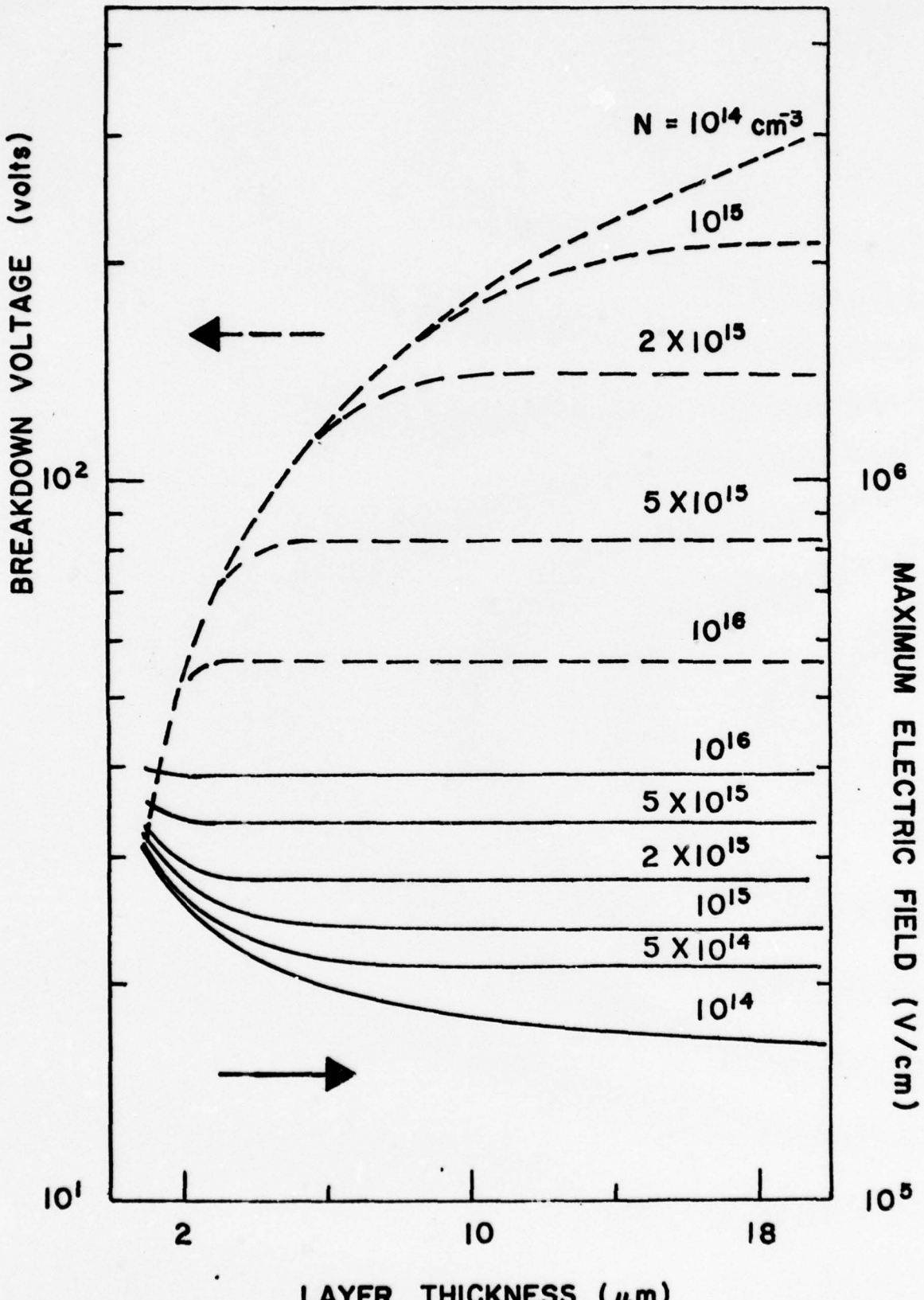

Fig. 2 Breakdown voltage and maximum electric field of GaAs EAP waveguide detectors as a function of layer thickness and doping level.

for holes, μ_j is the reduced mass, and the sum is over the light- and heavy-hole valence bands. In Fig. 3, the absorption coefficient for GaAs is plotted versus photon wavelength for various values of electric field. The following values for GaAs were used in calculating the absorption coefficient:

$$M_{v_1}/M = 0.067,\ M_{v_2}/M = 0.45,\ M_e/M = 0.067,\ \mu_j = \frac{M_e M_{v_j}}{M_e + M_{v_j}},$$

and the dispersion of the refractive index for GaAs

$$n(\lambda) = \left[8.950 + 2.054\left(\frac{\lambda^2}{\lambda^2 - 0.390}\right)\right]^{1/2}.$$

2.4 Waveguide Mode Absorption

The electroabsorption coefficient is not constant in the device because of the nonuniform electric field across the active region. If the absorption is small (the incident photon energy is less than the energy gap of GaAs), then perturbation theory can be applied to derive an equivalent electroabsorption coefficient for each guided wave propagating in the device.

In the following derivation we assume that for the transverse field distribution of the guided modes propagating along the device, only the field amplitude is decreased due to electroabsorption. Also, we assume that the photon energy of the guided waves is less than the energy gap of GaAs. Let the photon flux density of the guided mode entering the device at $Z = 0$ be denoted by $\phi_i(X) \equiv \phi(X,0)$. Then the photon flux density at position Z in the device is

$$\phi(X,Z) = A(Z)\phi_i(X), \qquad (2\text{-}10)$$

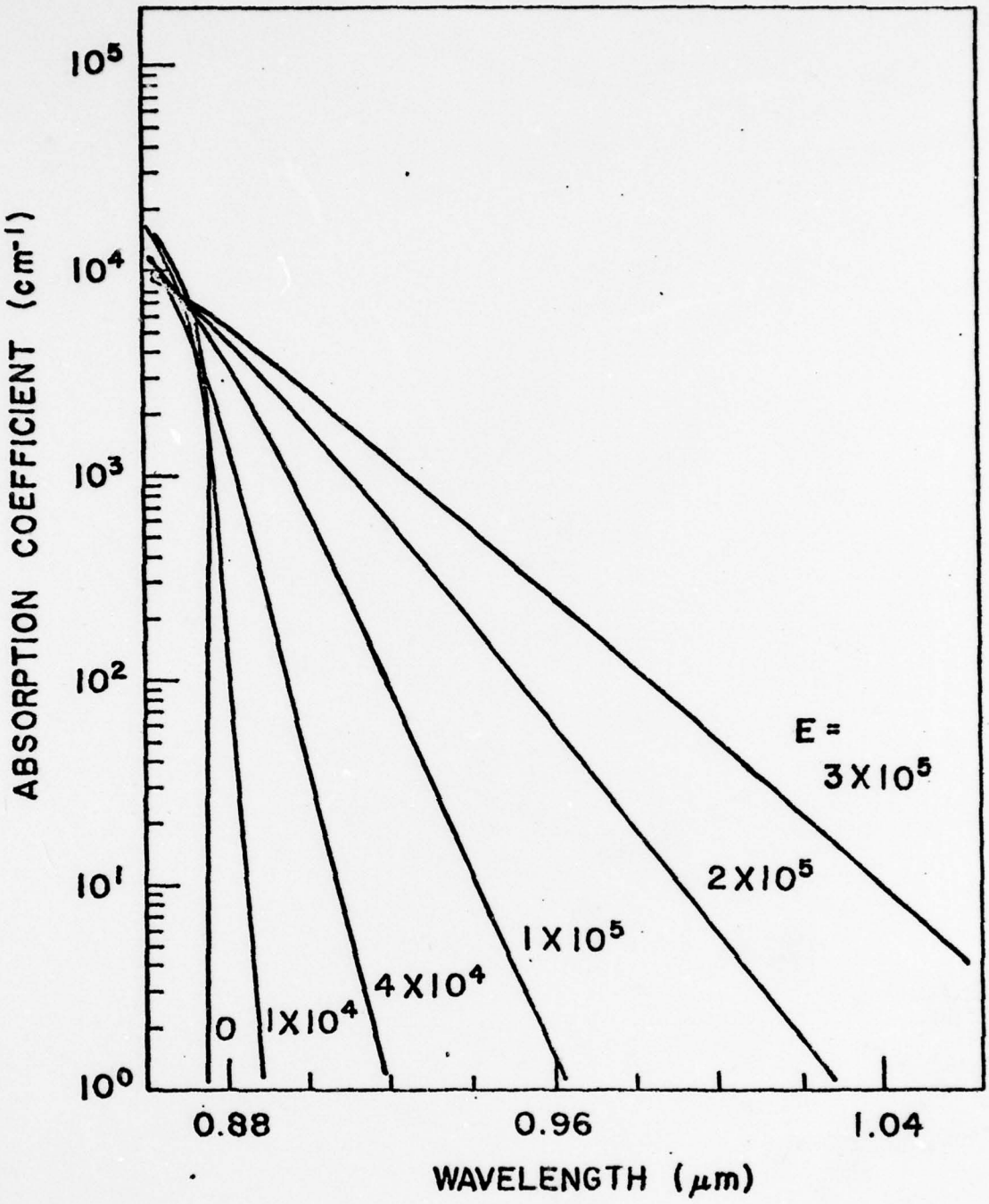

Fig. 3 Electroabsorption coefficient for GaAs as a function of wavelength for several values of electric field.

where A(Z) is a monotonically decreasing function of Z. The electroabsorption can also be expressed in terms of conductivity by using Maxwell's equations. That is,

$$\nabla \times \vec{H} = \frac{\partial \vec{D}}{\partial t}$$

$$= j\omega\varepsilon_0(\varepsilon' - j\varepsilon'')\vec{E}$$

$$= j\omega\varepsilon_0\varepsilon'\vec{E} + \sigma\vec{E},$$

when $\sigma \equiv \omega\varepsilon_0\varepsilon''$ is the equivalent conductivity in the lossy region, and ε', ε'' are the real and imaginary parts of the dielectric constant, respectively. Let the corresponding complex refractive index be $n = n' - jn''$. The field components of a plane wave propagating in the Z-direction in a infinite medium of refractive index n is proportional to this factor. That is,

$$e^{j(\omega t - nk_0 Z)} = e^{j(\omega t - n'k_0 Z)} e^{-n''k_0 Z}$$

$$= e^{-\frac{\alpha}{2}Z} e^{j(\omega t - n'k_0 Z)}$$

where $\alpha \equiv 2n''k_0$ in our case is the electroabsorption coefficient. On the other hand,

$$\varepsilon = \varepsilon' - j\varepsilon''$$

$$= (n' - jn'')^2$$

$$= n'^2 - n''^2 - 2jn'n'' .$$

So that

$$\varepsilon'' = 2n'n'' = n'\alpha/k_0,$$

and the equivalent conductivity in the lossy medium is given by

$$\sigma = \frac{\omega E_0 \, n'\alpha}{k_0}$$

$$\simeq \alpha n \sqrt{\frac{\varepsilon_0}{\mu_0}}, \quad (n'' << n').$$

The transverse electric field component of a guided mode can be expressed as

$$\vec{E} = \sqrt{A(Z)} \; \vec{E}_0(X) e^{-j\beta Z},$$

where $\vec{E}_0(X)$ is the original field component entering at $Z = 0$ which satisfies the normalization condition

$$\frac{1}{2} \int_{-\infty}^{\infty} (\vec{E}_0 \times \vec{H}_0^*) \cdot \hat{Z} dX = 1.$$

The power absorbed in a propagation distance between Z and Z + dZ in the device can be expressed as

$$\frac{dZ}{2} \int_0^{T,W} \sigma(X) \, |E(X,Z)|^2 dX$$

$$= \frac{dZ}{2} n \sqrt{\frac{\varepsilon_0}{\mu_0}} A(Z) \int_0^{T,W} \alpha(X) E_0^{\,2}(X) dX,$$

where the upper limit of integration is taken as the smaller of T and W. The incident photon flux density is given by

$$\phi(X,0) = \phi_i(X) = \frac{1}{2}(\vec{E}_0 \times \vec{H}_0) \cdot \hat{Z}/(hc/\lambda)$$

$$= \frac{\lambda}{2hc} \frac{\beta}{\omega\mu_0} E_0^{\,2}$$

so that the power absorbed in a distance between Z and Z + dZ is

$$\left(\frac{\omega \mu_0 hc}{\lambda \beta} \, n \sqrt{\frac{\varepsilon_0}{\mu_0}} \, A(Z) \int_0^{T,W} \alpha(X) \phi_i(X) dX \right) dZ. \qquad (2\text{-}11)$$

From Eq. (2-10) we find that

$$\frac{\partial \phi(X,Z)}{\partial Z} = \phi_i(X)\frac{dA(Z)}{dZ} \quad . \tag{2-12}$$

and the absorbed power between Z and Z + dZ is

$$\left(-\frac{hc}{\lambda} A'(Z) \int_{-\infty}^{\infty} \phi_i(X)\,dX\right)dZ \quad , \tag{2-13}$$

where the minus sign is obtained because A(Z) is a decreasing function of Z. From Eqs. (2-11) and (2-13), we have

$$-A'(Z) \int_{-\infty}^{\infty} \phi_i(X)\,dX = \frac{\omega\mu_0 n\sqrt{\frac{\varepsilon_0}{\mu_0}}}{\beta} A(Z) \int_0^{T,W} \alpha(X)\,\phi_i(X)\,dX$$

$$= \frac{n}{\beta/k_0} A(Z) \int_0^{T,W} \alpha(X)\,\phi_i(X)\,dX,$$

or

$$A'(Z) = -\frac{\frac{n}{\beta/k_0}\int_0^{T,W} \alpha(X)\,\phi_i(X)\,dX}{\int_{-\infty}^{\infty} \phi_i(X)\,dX} A(Z) \quad .$$

Therefore, $A(Z) = ce^{-\int_0^Z \Gamma dZ}$, where

$$\Gamma = \frac{n}{\beta/k_0} \int_0^{T,W} \alpha(X)\,\phi_i(X)\,dX \Big/ \int_{-\infty}^{\infty} \phi_i(X)\,dX$$

$$\Gamma = \frac{n}{\beta/k_0} \frac{hc}{\lambda} \int_0^{T,W} \alpha(X)\,\phi_i(X)\,dX \tag{2-14}$$

Since at Z = 0, A = 1, the integration constant C = 1, and the solution for A(Z) becomes

$$A(Z) = e^{-\Gamma Z}.$$

The photon flux density of the guided wave propagating in the device can thus be written as

$$\phi(X,Z) = \phi_i(X)e^{-\Gamma Z} ,$$

where the constant Γ is defined as the equivalent electro-absorption coefficient for guided waves propagating in the device. From Eq. (2-14), we can see that Γ equals the Franz-Keldysh electroabsorption coefficient for a given value of electric field only when $\alpha(X)$ is a constant and $\beta/k_0 = n$: that is, when all the guided energy is contained inside the guiding layer. In the waveguide structure considered here the refractive indices of the guiding layer and substrate differ by a very small amount (less than 0.1%), so that $\beta/k_o \simeq n$. The difference between Γ and α arises only from the nonuniformity of α in the depletion layer. For higher purity layers (N less than $10^{14}cm^{-3}$), $\Gamma \simeq \alpha$ since the almost uniform electric field in the depletion region (pinch-through) gives approximately uniform absorption.

In Fig. 4, calculated values of the equivalent absorption coefficient Γ at $\lambda = 0.905\mu m$ are plotted against bias voltage for three guided TE-modes. The calculation is based on a doping density for the layer of $5 \times 10^{15}cm^{-3}$ and for the substrate, $10^{18}cm^{-3}$. The layer thickness was $10\mu m$. This waveguide structure can support three TE and three TM modes. The breakdown voltage was calculated to be 88V from ionization coefficient data.[4] Other values used in the calculation were

The photon flux density of the guided wave propagating in the device can thus be written as

$$\phi(X,Z) = \phi_i(X)e^{-\Gamma Z} ,$$

where the constant Γ is defined as the equivalent electroabsorption coefficient for guided waves propagating in the device. From Eq. (2-14), we can see that Γ equals the Franz-Keldysh electroabsorption coefficient for a given value of electric field only when $\alpha(X)$ is a constant and $\beta/k_0 = n$: that is, when all the guided energy is contained inside the guiding layer. In the waveguide structure considered here the refractive indices of the guiding layer and substrate differ by a very small amount (less than 0.1%), so that $\beta/k_o \simeq n$. The difference between Γ and α arises only from the nonuniformity of α in the depletion layer. For higher purity layers (N less than $10^{14}cm^{-3}$), $\Gamma \simeq \alpha$ since the almost uniform electric field in the depletion region (pinch-through) gives approximately uniform absorption.

In Fig. 4, calculated values of the equivalent absorption coefficient Γ at $\lambda = 0.905\mu m$ are plotted against bias voltage for three guided TE-modes. The calculation is based on a doping density for the layer of $5 \times 10^{15}cm^{-3}$ and for the substrate, $10^{18}cm^{-3}$. The layer thickness was $10\mu m$. This waveguide structure can support three TE and three TM modes. The breakdown voltage was calculated to be 88V from ionization coefficient data.[4] Other values used in the calculation were

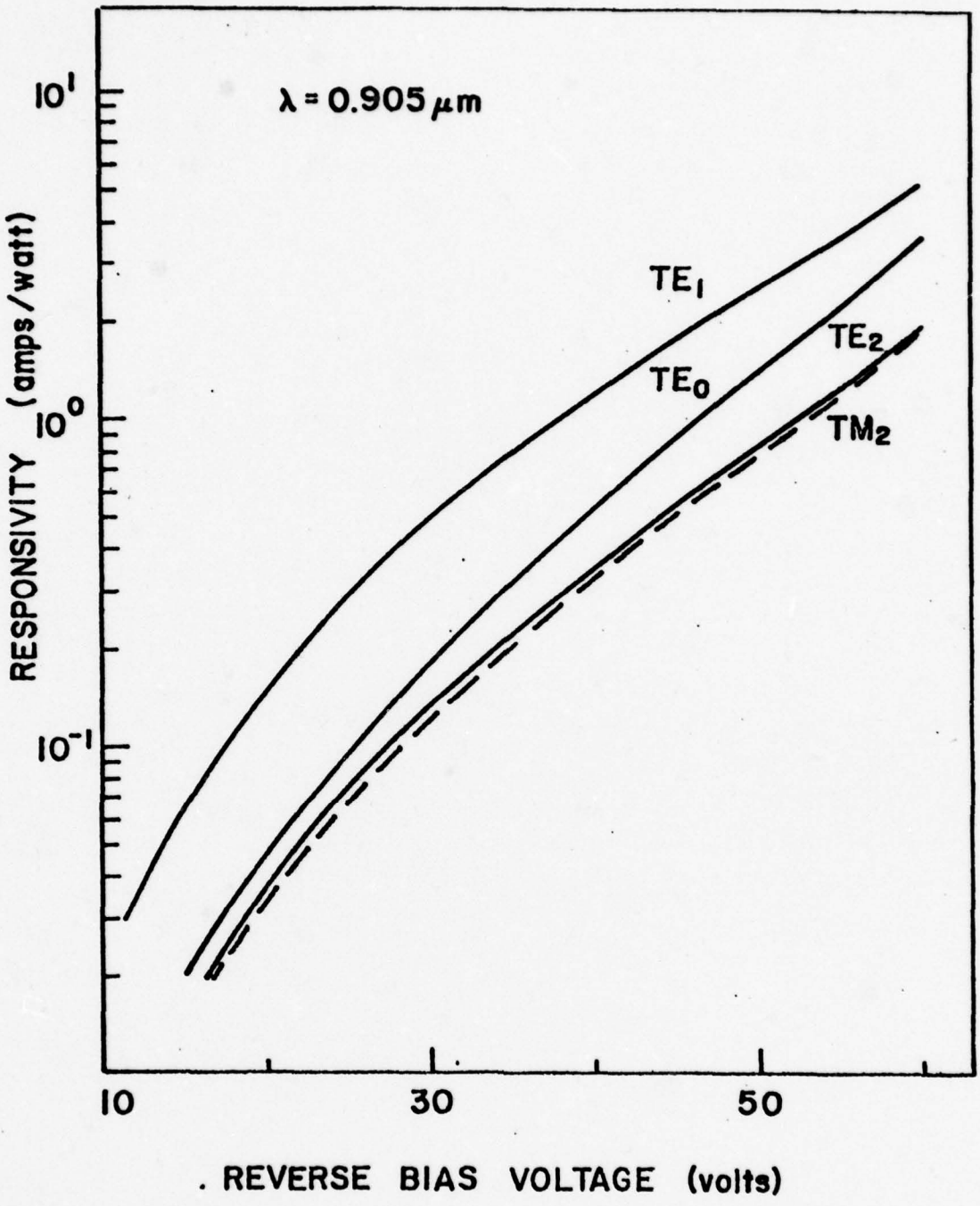

Fig. 4 Calculated equivalent absorption coefficient as a function of reverse bias voltage for several waveguide modes at 0.905μm. The device is assumed to be doped at $5\times10^{15}cm^{-3}$ in a 10μm thick waveguide on a $10^{18}cm^{-3}$ substrate. The breakdown voltage is 80 volts.

an electron effective mass of $0.067\,M_o$, light and heavy hole masses of $0.067\,M_o$ and $0.45\,M_o$, respectively, an energy gap of 1.42 eV, and a static dielectric constant of 12.53.

2.5 Quantum Efficiency and Responsivity

The differential equations for current density in the device can be expressed as

$$\frac{\partial J_n(X,Z)}{\partial X} = \alpha_n(X) J_n(X,Z) + \beta_p(X) J_p(X,Z) + qG(X,Z),$$

$$\frac{\partial J_p(X,Z)}{\partial X} = -\frac{\partial J_n(X,Z)}{\partial X}, \qquad (2\text{-}15)$$

where

$$J_n(X,Z) + J_p(X,Z) = J(Z),$$

$G(X,Z)$ = generation rate of photon-excited electron-hole pairs

$$= -\frac{\partial \phi(X,Z)}{\partial X},$$

$\phi(X,Z)$ = photon flux density

$$= \phi_i(X) e^{-\Gamma Z},$$

$\phi_i(X)$ = incident photon flux density, and

Γ is given by Eq. (2-14). $G(X,Z)$ can be written as

$$G(X,Z) = \alpha(X)\phi_i(X)e^{-\Gamma Z}.$$

From Eq. (2-15), we obtain

$$J_n(X,Z) = \left[\int_0^X (J(Z)\beta_p(X') + qG(W,X';Z)) e^{-\int_0^{X'} (\alpha_n - \beta_p) dX''} dX' + J_n(0,Z)\right] \Big/ e^{-\int_0^X (\alpha_n - \beta_p) dX'}.$$

Then since $J_n(X,Z) = J(Z) - J_p(X,Z)$, we obtain

$$J(Z) = \left[q \int_0^{T,W} G(W,X,Z)\, e^{-\int_0^X (\alpha_n - \beta_p)dX'} dX + J_n(0,Z) \right.$$

$$\left. + J_p(W,Z) e^{-\int_0^{T,W} (\alpha_n - \beta_p)dX} \right] \Bigg/ \left[e^{-\int_0^{T,W} (\alpha_n - \beta_p)dX} \right.$$

$$\left. - \int_0^{T,W} \beta_p(X)\, e^{-\int_0^X (\alpha_n - \beta_p)dX'} dX \right] ,$$

where again the upper limit of integration is the smaller of T or W. The total photocurrent is

$$I_{ph} = h \int_0^L J_{ph}(Z)\, dZ$$

$$= \left[qh \left(\frac{1 - e^{-\Gamma L}}{\Gamma} \right) \int_0^{T,W} \alpha(X) \phi_i(X)\, e^{\int_X^{T,W} (\alpha_n - \beta_p)dX'} dX \right]$$

$$\Bigg/ \left[1 - \int_0^{T,W} \beta_p(X) e^{\int_X^{T,W} (\alpha_n - \beta_p)dX'} dX \right] .$$

The internal quantum efficiency is given by

$$\eta \equiv \frac{I_{ph}}{qh \int_{-\infty}^{\infty} \phi_i(X)dX}$$

$$= \left[\left(\frac{1 - e^{-\Gamma L}}{\Gamma} \right) \int_0^{T,W} \alpha(X) \phi_i(X) - e^{\int_X^{T,W} (\alpha_n - \beta_p)dX'} dX \right]$$

$$\Bigg/ \left[\left(1 - \int_0^{T,W} \beta_p(X) e^{\int_X^{T,W} (\alpha_n - \beta_p)dX'} dX \right) \int_{-\infty}^{\infty} \phi_i(X)dX \right] .$$

The responsivity is then determined from the internal quantum efficiency as

$$R = \frac{\lambda}{1.24} \eta \text{ (amp/watt)}$$

where λ is the photon wavelength in microns.

Fig. 5 shows the calculated responsivity of an EAP waveguide detector as a function of applied bias for several 0.905μm waveguide modes. These calculated values are for a device with a doping level of $5 \times 10^{15} cm^{-3}$, a substrate doping level of $10^{18} cm^{-3}$, a layer thickness of 10μm, and a device length of 100μm. Since the electroabsorption coefficient varies with polarization, a somewhat different expression must be used for TM waves. When comparing these calculated curves to experimental values, an average must be taken of the calculated curves since the device does not distinguish between waveguide modes.

3. FABRICATION

3.1 Epitaxial Layers

The epitaxial layers for the waveguide and active region of the GaAs EAP detectors are grown in an $ASCl_3$-Ga-H_2 vapor-phase reactor shown schematically in Fig. 6. Hydrogen is used as a carrier gas and is purified with a palladium diffusion cell. The source of arsenic and chlorine is $AsCl_3$ which is kept in a quartz bubbler surrounded by a water bath. The water bath is attached to a constant temperature refrigerated circulator. Elemental gallium is placed in a 3" Spectrosil boat which, in turn, is placed in the furnace tube from the 17"

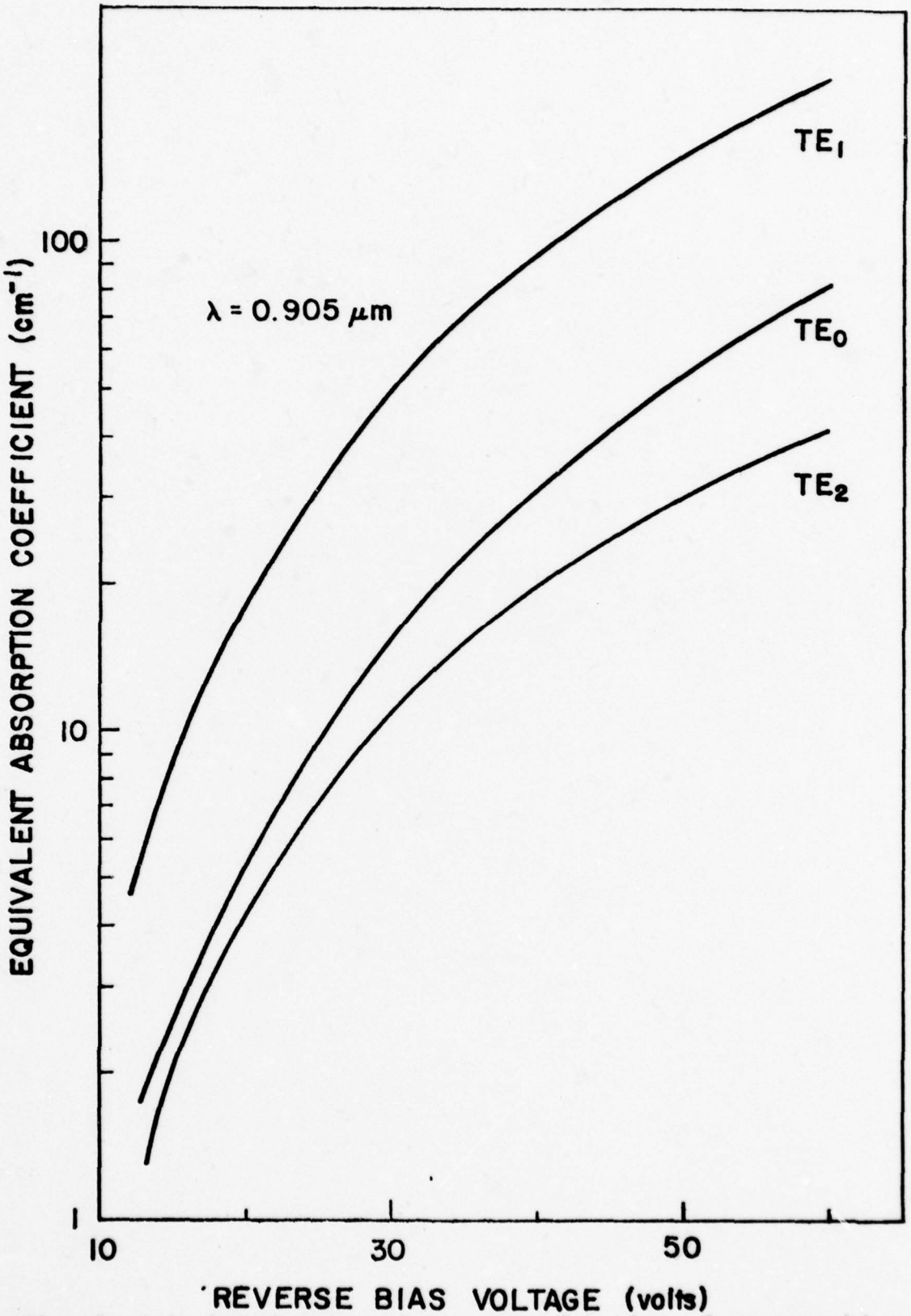

Fig. 5 Calculated responsivity as a function of reverse bias voltage for several waveguide modes at 0.905μm. The device parameters are the same as in Fig. 4.

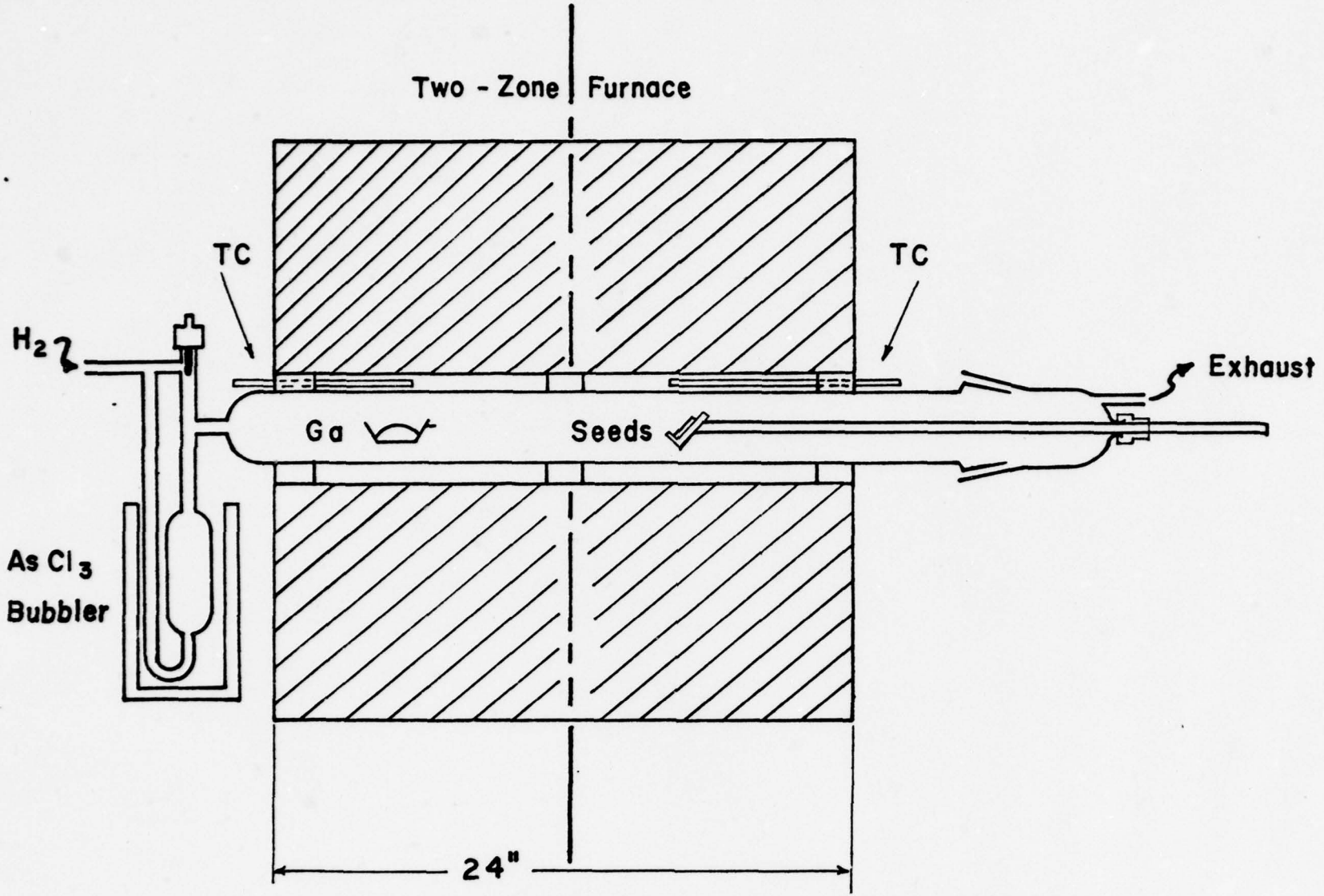

Fig. 6 Schematic of the epitaxial reactor used to grow GaAs layers.

to 20" points (distances measured from the right-hand side of the furnace). Across this distance the temperature is almost constant with a 3^{o} to 4^{o}C differential from the end points to the middle. The gallium used is semiconductor grade produced by Alusuisse with a purity of 99.9999+%.

To control the doping of the epitaxial layers tin spheres are added to the gallium melt. With 20 gms of gallium and the $AsCl_3$ temperature set at 8^{o}C, four 10 mil Sn spheres yield a doping level between 5×10^{14} and $1 \times 10^{15} cm^{-3}$. Five 10 mil Sn spheres produce a doping level of 2×10^{15} to $7 \times 10^{15} cm^{-3}$ while six 10 mil Sn spheres give 8×10^{15} to $2 \times 10^{16} cm^{-3}$. For unguarded Schottky barrier devices the desired doping level is usually in the upper $10^{14} cm^{-3}$ range.

The reactor tube is made of fused quartz and can be opened at one end through a taper joint on which is mounted the seed holder. The system is air tight to prevent contamination and is centered in the furnace by wrapping asbestos tape around the tube. The furnace is a Marshall Model 1137S which is wired to produce two zones. Each zone is controlled by LFE solid state controllers (Model 226). The zone from 24" to 12" controls the temperature of the gallium melt which is kept at $840\ ^{o}$C. Feedback is provided by a chromel-alumel thermocouple at 18". The second zone (12"-0") controls the temperature of the substrates. The position of the feedback thermocouple can be varied to change the temperature gradient across the sample. The seed holder and thermocouple are at the 5" point which results in a gradient of 10^{o}C per inch across the substrates.

Before epitaxial growth is attempted the gallium melt is saturated with arsenic until a GaAs skin is produced over the gallium. When a new gallium melt is put into the reactor the furnace is preheated for 2 hours with the first temperature controller set at 840 ^{0}C and the second controller set at 805^{o}C. After the preheat the hydrogen is bubbled through the $AsCl_3$ at a rate of 150 ml/min. The temperature of the $AsCl_3$ is set at either 8^{o} or 9^{o}C depending on the temperature desired for epitaxial growth. These temperatures and flow rate are maintained for three hours, then the second temperature controller is changed to 750 ^{o}C. After three hours of saturation under these conditions, the $AsCl_3$ is turned off and the hydrogen flow lowered to 30 ml/min. The furnace is then shut off and left to cool overnight.

The epitaxial layers for the EAP detectors are grown on tellurium-doped substrates from Laser Diode Laboratories. They typically have a resistivity of 0.0018 ohm-cm and a doping level of $1.6 \times 10^{18} cm^{-3}$. The crystallographic orientation is two degrees off the {100} planes to prevent the formation of hillocks. Layers are simultaneously grown on chromium-doped substrates to determine carrier concentration, mobility, and ionized donor and acceptor concentrations.[6] The electrical characteristics of the epitaxial layer grown on a chromium substrate should be the same as the epitaxial layer grown on a n^{+} substrate when they are grown together. The resistivity of the substrates grown by Laser Diode Laboratories is about 2×10^{7}ohm-cm, with

a crystallographic orientation of {100}. To remove saw damage the substrates are first mechanically-chemically polished with a 1% bromine-methanol solution. This is sprayed on a napless nylon mat attached to a polishing wheel. After polishing the wafers are typically 10 to 15 mils thick.

Just before use the substrates are cleaved into the desired size and cleaned with organic solvents in a quartz beaker. Hot trichloroethylene, acetone, and methanol in sequence are used for this purpose. The beaker is then moved under a dust-free hood where the sample is dried with bibulous paper. The sample is then etched in a $5H_2SO_4:1H_2O_2:1H_2O$ solution. This etchant is first cooled for 5 minutes after mixing, while it is being stirred. The substrates are then put in the etchant and stirred for another 5 minutes. Without exposing them to air, the substrates are then rinsed in deionized water, put under the dust-free hood, and dried with bibulous paper.

After etching the substrates are placed on the seed holder and inserted in the furnace. The reactor is then flushed with hydrogen for 15 to 20 minutes at a flow rate of 250 ml/min. The furnace is then turned on and preheated for two hours. The first temperature controller is set at 840°C and the second controller is set at 700°C with a flow of 50 ml/min of hydrogen. The seeds are heated to 700°C to minimize the arsenic loss from the substrates. After this preheat the second temperature controller is raised to 730°C. Within 15 min. the temperature has stabilized, and it is then raised to 750°C. When the temperature

has stabilized (15 min.) the hydrogen flow is raised to 150 ml/min, and the by-pass is closed so the hydrogen will bubble through the $AsCl_3$. The $AsCl_3$ is maintained at 8^oC to help suppress the formation of hillocks. Under these conditions a growth rate of 5 microns per hour is obtained.

For unguarded EAP detectors the thickness of the epitaxial layer is between 5 to 15 microns, which can be attained in a growth time between one and three hours. After the desired time the hydrogen by-pass is opened, and the hydrogen flow is reduced to 30 ml/min. The furnace is turned off and left to cool for at least 6 hours. To measure the thickness after the samples are removed from the furnace, thin slices are cleaved from the top and bottom of the sample. These slices are placed in a solution of $1HF:3HNO_3:4H_2O$ for about 10 sec., which delineates the epitaxial layer-substrate interface, and then rinsed in deionized water. These slices are then placed under a microscope and visually measured with a calibrated eyepiece.

3.2 Ohmic Contacts

When the desired doping level and thickness have been achieved, the next step is to make an ohmic contact to the n^+ substrate. Usually to facilitate cleaving the back of the sample is lapped with 5 micron grit to remove growth on the back of the sample. The sample is cleaned in hydrofluoric acid, hydrochloric acid, and rinsed in deionized water.

After drying the sample, it is placed in a pyrolytic SiO_2 reactor with the epitaxial layer up. The nitrogen flow through one inlet is 4 liters/min with 10 ml/min of silane added. The sample is heated to 300°C and a flow of 4 liters/min of nitrogen with 40 ml/min of oxygen is turned on in a second inlet. Under these conditions a SiO_2 layer 4400 Å thick is deposited in four to six minutes, and the reaction is halted. This SiO_2 layer is used to protect the GaAs epitaxial surface while fabricating the ohmic contact.

To obtain a plating contact a small hole is made in the SiO_2 through to the GaAs near one edge. The sample is placed on the heating strip of an alloying station and a 20-mil Sn sphere is alloyed in the hole. The heating strip is isolated from the atmosphere and 350 ml/min of high purity hydrogen with 200 ml/min of hydrogen chloride is allowed to flow through the system to reduce oxides on the Sn spheres and GaAs surface and improve the alloying. The sample is slowly heated to 280°C, then cooled with the hydrogen chloride off. A five inch length of indium-plated nickel ribbon is attached to the alloyed Sn sphere. The sample is then mounted face down on one end of a microscope slide with black wax. When mounting the wire is drawn along the microscope slide and completely covered with black wax except for a small tail protruding beyond the slide. This insulation of the wire is necessary to allow most of the plating current to pass through the sample.

The electroplating solution used for the ohmic contact is a Technic Au-Sn solution. This solution is heated to a temperature between 55^{o} and $60^{o}C$ and a current density of $20ma/cm^{2}$ is used. The area of the sample is measured, and the current needed to produce this current density is calculated. To produce this current a constant current source is used. The positive terminal is connected to a 316 stainless steel anode immersed in the solution while the negative terminal is attached to the tail of the nickel ribbon. The sample is then immersed in the solution which is vigorously stirred, and the current is applied. After 30 seconds the sample is removed and immediately rinsed in deionized water. The sample is then removed from the slide by dissolving the black wax in trichloroethylene.

The nickel ribbon and excess tin are removed with a soldering iron. The sample is placed face down on the carbon heating strip of the alloying station. The station is sealed, and a hydrogen flow of 350 ml/min is introduced. After a 10 min flush the heat is turned to a maximum. When the temperature reaches between $480^{o}C$ and $500^{o}C$ the gold-tin, which is a light gold after plating, diffuses in and the surface becomes a light gray. At this point the power is immediately turned off. This alloying usually takes between 10 and 30 seconds. This procedure produces very low resistance contacts to the n^{+} substrate.

3.3 Schottky Barriers

To make aluminum Schottky Barriers the sample is first cleaned in hydrofluoric acid to remove the SiO_2 layer on the epitaxial layer. It is then rinsed in deionized water and cleaned in hydrochloric acid. After rinsing in deionized water and drying, the ohmic contact on the back of the sample is covered with SiO_2. The procedure is the same as described for making the protective layer for the Au-Sn plating. The sample is again cleaned in the organic solvents, trichloroethylene, acetone, and methanol. To increase the adherence of the aluminum on the GaAs, the epitaxial surface is etched just before the sample is mounted in the evaporation system. The etchant is $5H_2SO_4:1H_2O_2:1H_2O$ which is cooled for 9½ minutes. The sample is then etched for 30 seconds and rinsed in deionized water making sure the sample is not exposed to air. After the sample is dried, it is mounted on the sample plate of an evaporation system. The sample plate is mounted and the bell jar lowered. The vacuum system is then pumped to a pressure of about 5×10^{-7} Torr at which time evaporation proceeds. The source is slowly heated until the Al melts, the shutter is opened, and the thickness monitored with a transducer mounted close to the samples. The shutter is closed after the desired thickness, usually 5000 Å, is reached.

Next the samples are removed from the evaporator, and the aluminum is covered with a layer of pyrolytically deposited SiO_2 (4400 Å) to be used as an etchant mask as in Fig. 7(a).

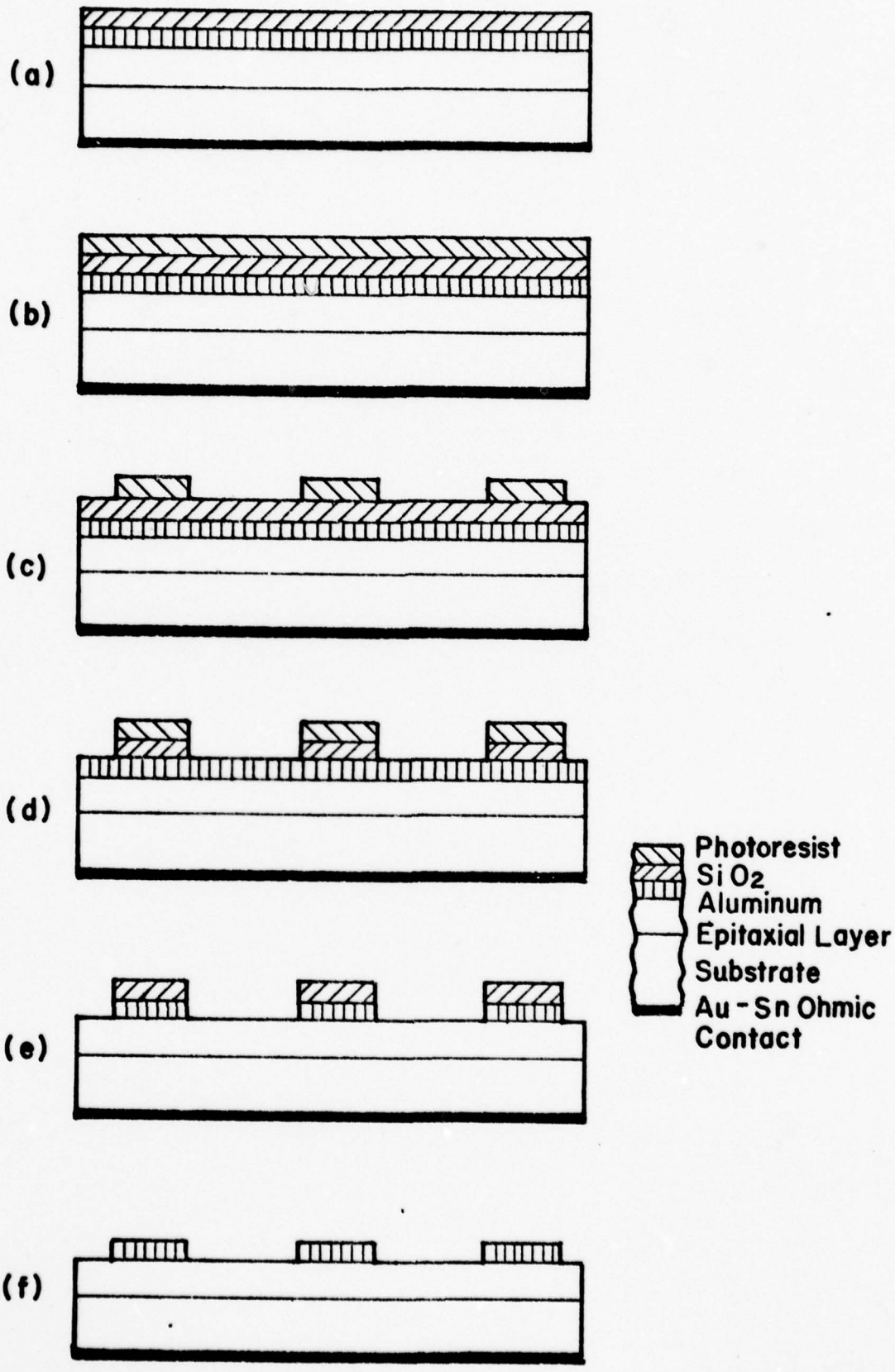

Fig. 7 Process used to fabricate GaAs EAP detectors with aluminum Schottky barriers.

To pattern the SiO_2 a layer of photoresist is spun on the SiO_2 as shown in Fig. 7(b) and developed selectively with a photolithographic mask. The photoresist used is AZ1350B which is filtered with a 0.2μm millipore filter mounted on a syringe. The filtered photoresist on the sample is spun at 3000 rpm for 30 seconds. The photoresist is then prebaked for 20 minutes at 70°C. An optical mask aligner is then used to expose the photoresist except for a pattern of 4-mil discs on 15-mil centers. This pattern is aligned along a cleavage plane with the x, y and θ controls while the sample is at a 4-mil separation from the mask. The mask is then pressed against the sample with about 2 lbs. of force, and the photoresist is exposed for 7 seconds. The exposed photoresist is developed with a 50% solution of Azoplate and deionized water. This solution is sprayed on the sample for 45 seconds and then rinsed in deionized water for another minute. The resulting structure, shown in Fig. 7(c), is dried and postbaked for one hour at 100°C.

The exposed SiO_2 is etched in buffered HF. The sample is immersed for 1 to 1½ min at room temperature to etch 4400 Å of SiO_2, then rinsed in deionized water. This etchant also attacks the aluminum; however, it is very slow and only etches the exposed surface slightly.

The etchant for the aluminum is Aurostrip diluted in deionized water to a concentration of 4 oz/gal. This concentration will develop the photoresist; so the sample (Fig. 7(d)) is first cleaned in acetone which removes the photoresist. The Aurostrip

solution is heated to between 45°C to 50°C. The higher temperature gives a slightly faster etch rate, 2500 Å/min compared to 2000 Å /min at 45°C. The sample is immersed until all of the aluminum is etched except that under the 4-mil discs to obtain the structure of Fig. 7(e). The SiO_2 mask then is removed in buffered HF and rinsed in deionized water. This yields the aluminum Schottky barrier EAP detector structure shown in Fig. 7(f).

If it is desired to fabricate gold Schottky barriers instead of aluminum, a somewhat different procedure is used. The protective SiO_2 layer used during the fabrication of the ohmic back contact is not etched off the epitaxial surface after the alloying of the Au-Sn (Fig. 8(a)). Instead this layer will be used as a gold Au plating mask. Photoresist is applied as described previously (Fig. 8(b)), however, the 4-mil discs on 15-mil centers are exposed instead of the area around them (Fig. 8(c)). This mask is the inverted image of the mask used for making aluminum Schottky barriers. The photoresist is developed in the same way and again is baked for 1 hour at 100°C. The SiO_2 is etched for 1 to 1½ minutes in buffered HF and rinsed in deionized water to obtain the structure shown in Fig. 8(d). After the patterning of the SiO_2 the photoresist is removed in acetone.

The plating of the gold on the epitaxial layer is similar to the plating of the Au-Sn for the ohmic contact on the substrate. The indium-plated nickel ribbon is pressure contacted

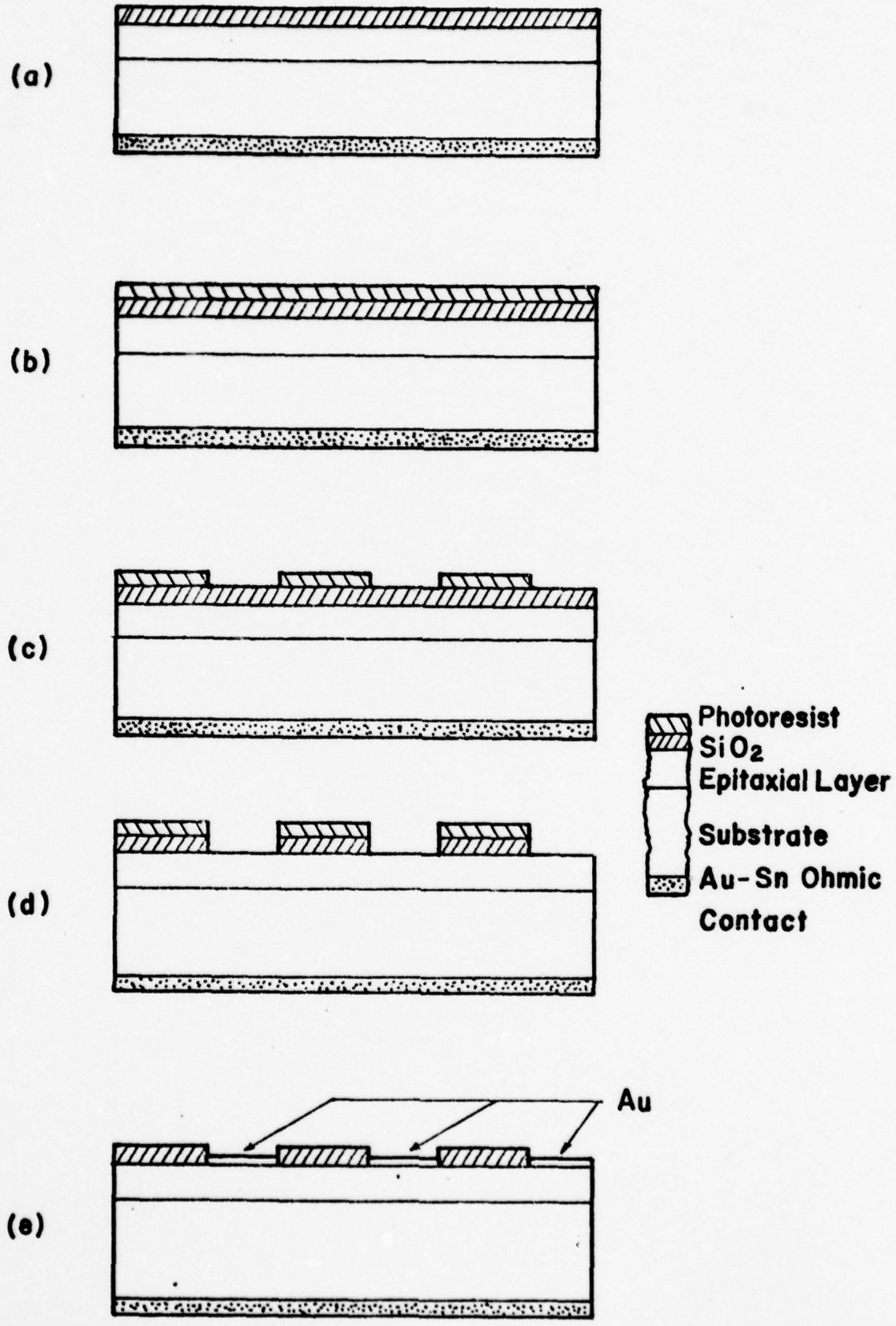

Fig. 8 Process used to fabricate GaAs EAP detectors with gold Schottky barriers.

on the ohmic contact with a small piece of indium. This indium is pressed on top of the nickel ribbon which is placed across the ohmic back surface. The sample is then placed on a microscope slide with black wax just as in the Au-Sn plating, however, in this case the masked epitaxial layer is now face up. The gold plating solution is Techni-Gold 25 made by Technic Inc. This solution is heated to a temperature between 48°C and 50°C. Before the sample is placed into the solution, the exposed surface is etched slightly to ensure a clean surface for the Schottky barrier. This is done by mixing $5H_2SO_4:1H_2O_2:1H_2O$ and letting it cool for 10 minutes. The sample is then etched for 10 sec and rinsed in deionized water. The sample is blown dry with nitrogen and immersed in the plating solution. The area to be plated has been calculated, and the constant current supply is set to give a current density of 3.25 ma/cm^2. The positive terminal is connected to a 316 stainless steel anode in the solution while the negative terminal is connected to the nickel ribbon. The current is turned on for one minute while the solution is vigorously stirred. The sample is then rinsed in deionized water and removed from the microscope slide in trichloroethylene. For this plating time the thickness of the gold Schottky barrier is 2000 Å. This yields a final geometry for the gold Schottky barrier as detector shown in Fig. 8(e).

3.4 Guarded Structures

To make guarded Schottky barrier EAP detectors, the device material is grown using the procedure described in Section 3.1. While the carrier concentration of the unguarded devices was usually between 5×10^{14} - $1\times10^{15}cm^{-3}$ the carrier concentration of the device material in this case is in the 3×10^{15} - $7\times10^{15}cm^{-3}$ range. This was accomplished by adding five 10-mil Sn spheres to the gallium melt. The other change from the procedure previously described is that the thickness of the epitaxial layer is from 25 to 30 microns. After lapping the back of the substrate with 5-micron grit, the epitaxial layer is cleaned in HF and HCl with deionized water rinses. SiO_2 is pyrolytically deposited using the procedure described previously. This SiO_2 layer is usually 4400 Å thick and is deposited on top of the epitaxial layer.

Photoresist is then deposited on top of the SiO_2 layer. Using the photolithographic techniques described previously, the photoresist is patterned into an array of 4-mil discs with 15 mil centers. The SiO_2 is then etched in buffered HF producing an array of 4 mil discs of SiO_2 with the structure shown in Fig. 9(a). The sample is then etched in $5H_2SO_4:1H_2O_2:1H_2O$ to give the mesa structure of Fig. 9(b). The etchant is cooled for 6 to 7 min, and then the sample is etched for 10 min. The sample is rinsed in deionized water making sure that the sample is not exposed to air. After drying with bibulous paper, the sample is placed on a microscope slide and the depth of the

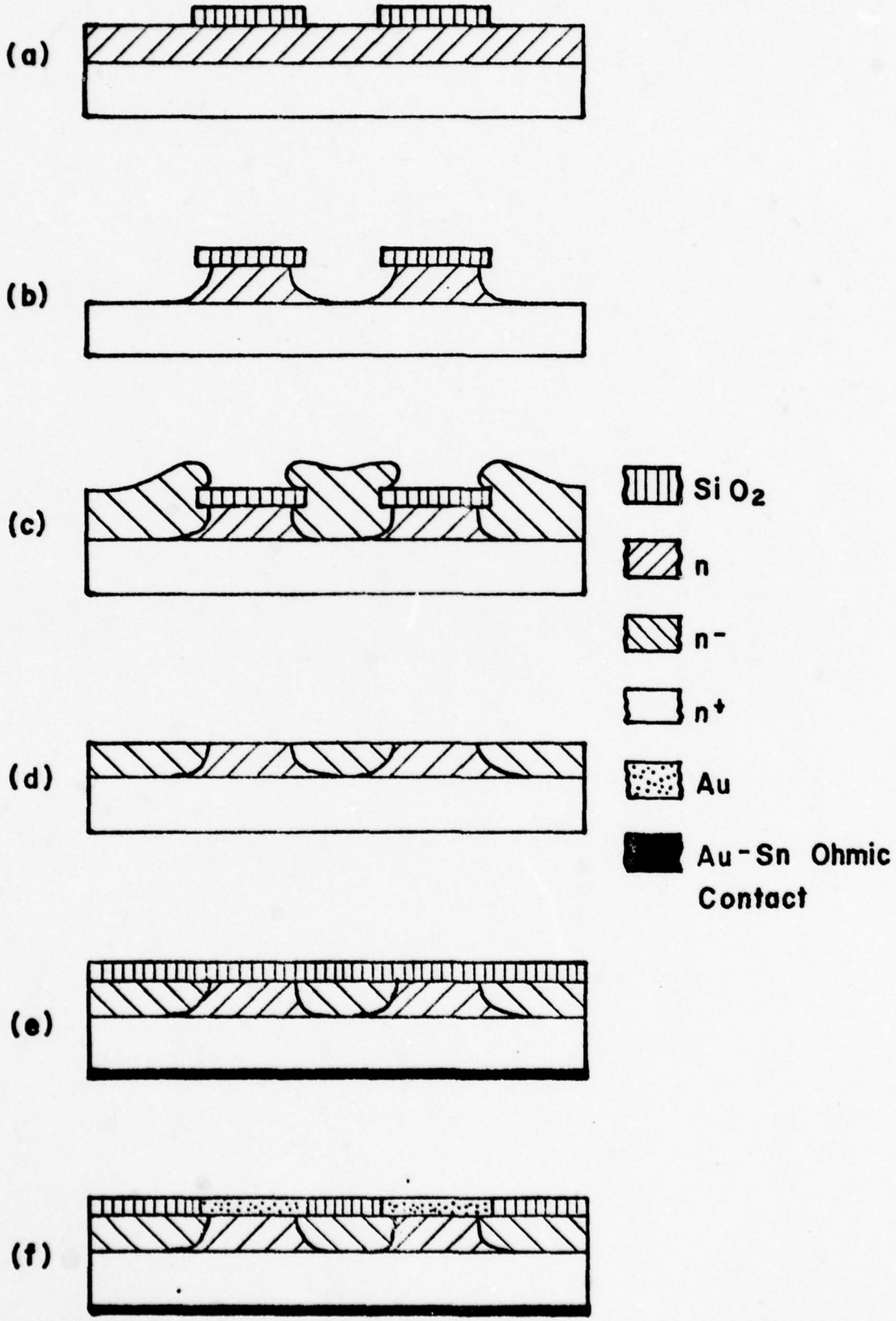

Fig. 9 Process used to fabricate guarded GaAs EAP waveguide detectors.

etching is measured with a microscope. The etching procedure described typically produces a depth of about 20 to 25 microns. The procedure is repeated if the etching is not through the epitaxial layer to the substrate.

The structure shown in Fig. 9(b) is then usually placed in the epitaxial reactor on the same day the mesas are etched. If they are left till the next day, the sample is etched for 30 sec after a 9½ min cool-down and then immediately put in the furnace. The reactor is then flushed for 15 to 20 minutes at a flow rate of 250 ml/min. The furnace is preheated for two hours with the melt temperature controller set at 840°C, and the seed controller set at 700°C with a flow of 50 ml/min of H_2. After the 2 hour preheat the temperature of the seeds is raised to 730°C and then to 750°C in 15 minute intervals. With the seed temperature at 750°C the H_2 by-pass is closed, and the H_2 is bubbled through the $AsCl_3$ at a rate of 150 ml/min.

The temperature of the $AsCl_3$ is set at 9°C to decrease the donor doping level of the epitaxial layer. The gallium melt is left undoped which, with an $AsCl_3$ temperature of 9°C, produces a high-resistivity layer. This resistivity is in the range of 100 to 1000 ohm-cm, which indicates a carrier concentration much less than that for the device mesa. This produces guarding since the reverse breakdown voltage is lower for the device mesa than for the high-resistance layer.[7] The growth time is chosen to be the same time used to grow the device material. This produces a slight overgrowth around the device

mesas as shown in Fig. 9(c). When the sample is removed from the reactor, the back of the sample is lapped with 5 micron grit. The SiO_2 is then removed with buffered HF. The sample is rinsed in deionized water, dried with bibulous paper, and mounted on a polishing block which has been ultrasonically cleaned.

The same procedure used to polish the substrates is used to flatten the sample surface, except that instead of the 1% bromine-methanol solution used for the substrates, a ½% bromine-methanol solution is used to reduce the etching rate. The sample is polished until the waveguide is between 5 to 10 microns. (Fig. 9(d)) At this point the back ohmic contact is fabricated with the process discussed in Section 3.2 and the Schottky barrier with one of the procedures indicated in Section 3.3. However, instead of 4-mil circles, 6-mil circles with 4-mil bounding pads are opened in the SiO_2. This produces the final EAP device structure shown in Fig. 9(f).

3.5 Packaging

To obtain packaged devices, the completed wafer discussed in Sections 3.3 and 3.4 with ohmic contacts and aluminum Schottky barriers are scribed into chips with approximately 3×3 GaAs EAP detectors per chip. The devices on each chip are probed to obtain a preliminary evaluation of the detectors and to select those which appear most suitable for further evaluation. These chips are then mounted on TO-18 headers in a hot stage with indium to alloy the substrate ohmic contact onto the header case.

A temperature of 200°C in the hydrogen-HCl atmosphere described in Section 3.2 is sufficient for this purpose. Finally, two of the best aluminum Schottky barriers on the epitaxial layer are ultrasonically bonded to the insulated posts on the header with 1-mil diameter aluminum wire.

Although this packaging process cannot be used for devices with gold Schottky barriers, it produces no degradation of detectors with aluminum Schottky barriers. In fact, the characteristics of the packaged EAP detectors with aluminum Schottky barriers are improved over the unpackaged devices because of their lower series resistance.

4. PERFORMANCE

The experimental set-up for measuring equivalent absorption coefficients and responsivity is shown in Fig. 10. Laser diodes of wavelength 0.905μm, and 0.915μm were used. A calibrated detector (lite-mike) was used to measure absolute power for the determination of detector responsivity.

4.1 Absorption at GaAs Laser Wavelengths

The equivalent absorption coefficient Γ is defined by

$$\phi(X,Z) = \phi_i(X)e^{-Z\Gamma}$$

where $\phi(X,Z)$ is the photon flux density. Thus, Γ can be calculated from measurements of the laser power radiated from the waveguide in which the detector is fabricated. Laser power is

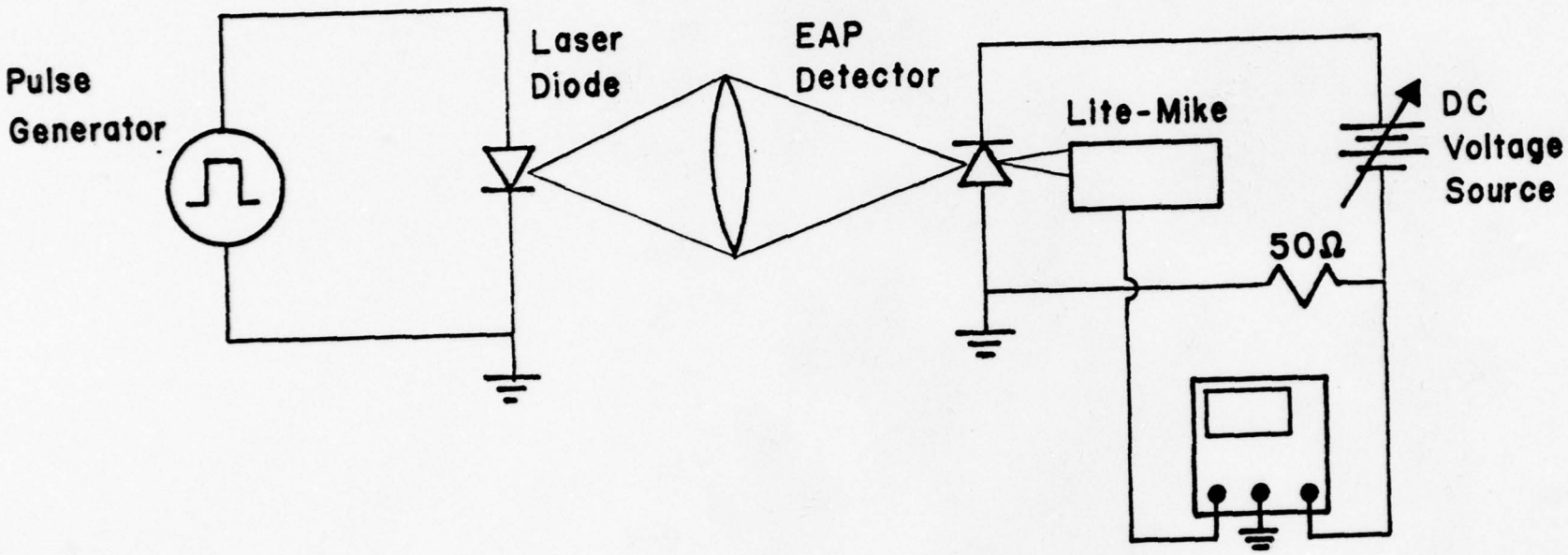

Fig. 10 Diagram of apparatus used to measure absorption and responsivity.

coupled into the waveguide by adjusting the position of the objective lens so that the laser beam is focused onto the front cleaved edge of the waveguide. Photocurrent is then generated in the detector by the absorption of laser power. The laser beam radiated from the back cleaved edge of the device is detected by the light-mike. With zero bias voltage on the EAP detector, the radiated power detected by the light-mike can be taken as the value of power incident on the EAP device, which is proportional to $\phi_i(X)$ (neglecting the absorption loss after the device). Then a bias voltage is applied to the EAP detector, and the corresponding output radiation is recorded, which is proportional to $\phi(X,L)$, when L is the detector length. Since

$$\Gamma = -\frac{1}{L}\ln\frac{\phi(X,L)}{\phi_i(X)} ,$$

then $\Gamma(V)$ can be determined from

$$\Gamma(V) \simeq -\frac{1}{L}\ln\frac{\phi_t(V)}{\phi_t(0)}$$

where ϕ_t is the total photon flux incident on the light-mike. Since only relative power values of output laser radiation from the waveguide are needed for calculating $\Gamma(V)$, no calibration is needed. Thus, a pulse amplifier can be used after the output detector (light-mike) if the signal is too small to be read accurately from the oscilloscope display. Such measurements were performed on several samples fabricated by different methods. Typically, these devices were 4-mils in diameter in 10μm

waveguides with doping levels of $5\times10^{15}cm^{-3}$ and breakdown voltages of around 80 volts.

Some of the data for these detectors are shown in Figs. 11 and 12 for laser wavelengths of 0.905 and 0.915μm, respectively. The data points in Figs. 11 and 12 are experimental values, while the solid lines are calculated electroabsorption values as in Fig. 4. As can be seen, there is reasonable agreement between the experimental and calculated data. On some samples microplasmas lower the breakdown voltage. With these devices the absorption increases much faster than that shown in Figs. 11 and 12 because the field in the microplasma regions are relatively high at low bias voltage.

4.2 Responsivity at GaAs Laser Wavelengths

Measurements of responsivity are less accurate than those of absorption because absolute values of the incident power to the device are required. The experimental arrangement is the same as that for the absorption measurements, except that the photocurrent in the EAP detector must also be determined. The magnitude of the photo-generated current is obtained by measuring the voltage across the 50-Ω resistor as shown in Fig. 10. Absolute incident power to the EAP detector was determined by measuring the total output radiated power from the waveguide with zero bias voltage and allowing for reflection loss at the output edge. The reflection at 0.905μm is about 0.32.

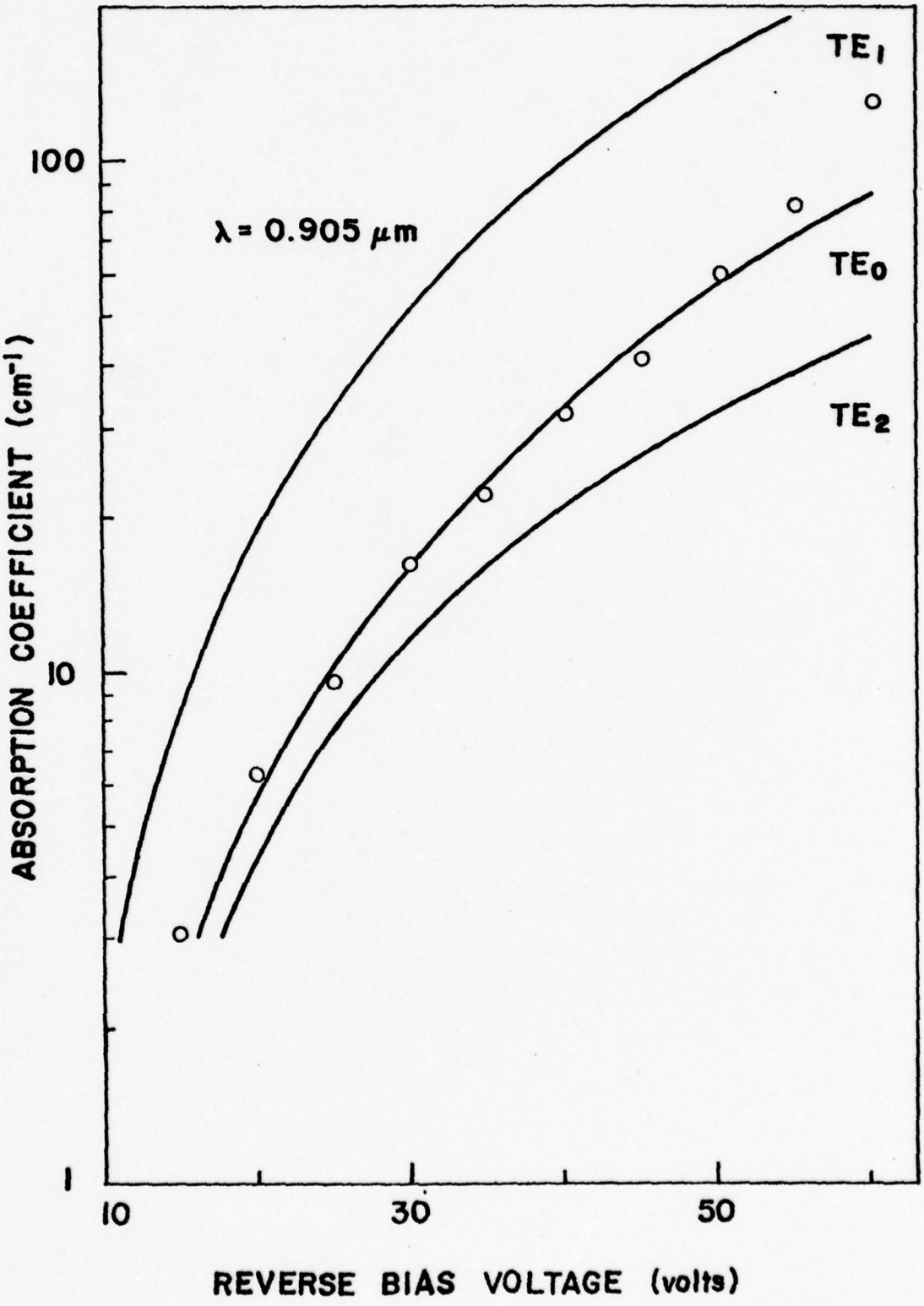

Fig. 11 Experimental absorption coefficient versus bias voltage at 0.905μm.

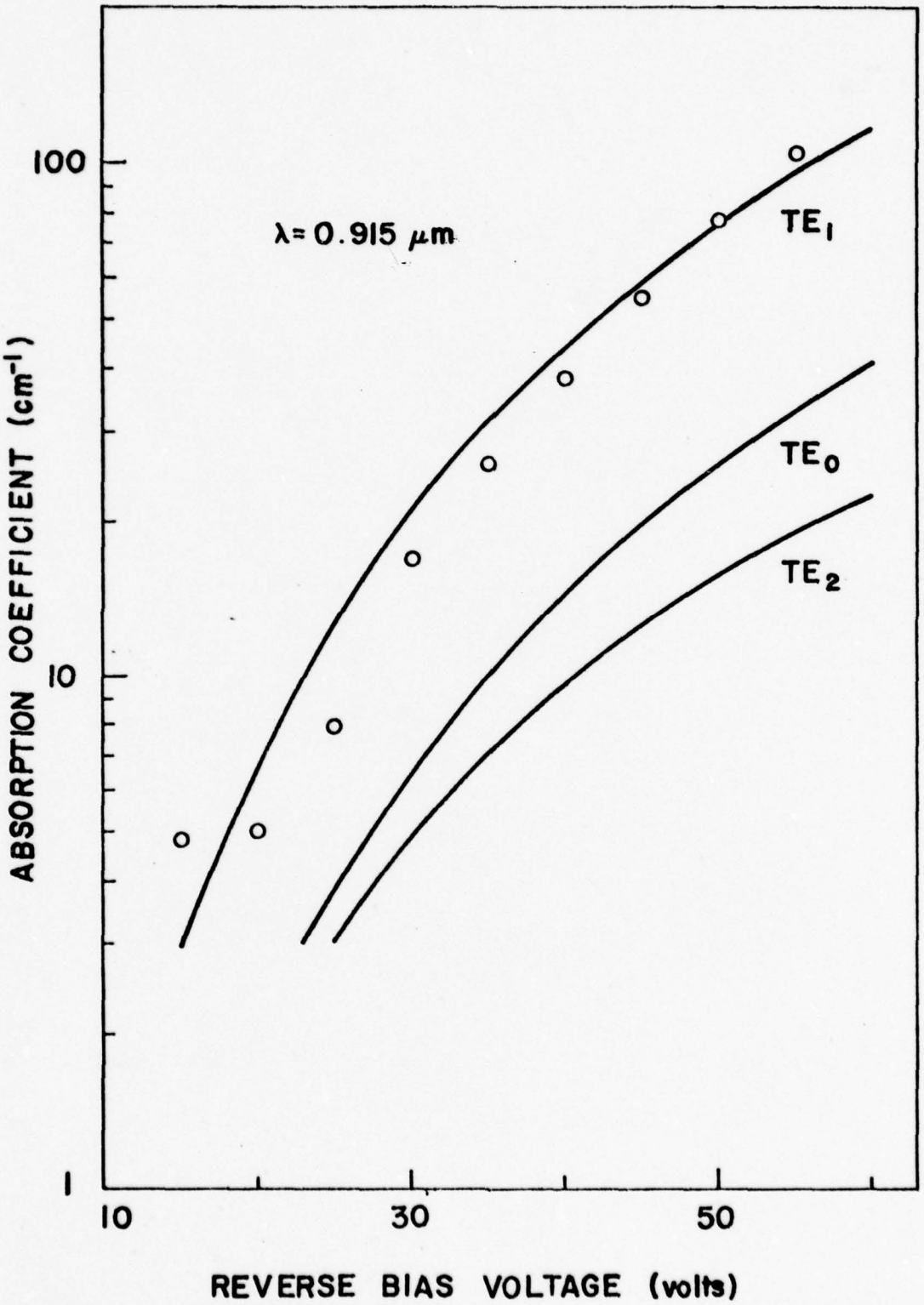

Fig. 12 Experimental absorption coefficient versus bias voltage at 0.915μm.

Figures 13 and 14 show responsivity curves as a function of reverse bias voltage for several EAP detectors at laser wavelengths of 0.905 and 0.915μm, respectively. The data points are experimental values while the solid lines are calculated responsivity curves as in Fig. 5. Parameters for the calculated curves were obtained from the doping level and thickness of the actual device. As can be seen the agreement between the calculated and experimental responsivity is not as good as the absorption data. The leveling off of the experimental responsivity at high bias voltages is probably due to the series resistance of the EAP detectors. Other differences may be caused by inaccuracy in determining absolute power or by not knowing the actual electric field distribution in the device.

4.3 Responsivity at 1.06μm

The responsivity of the GaAs EAP detectors was also measured at 1.06μm. Because of the lower absorption at this wavelength, however, a different geometry was employed. In this case the detector geometry was a long thin rectangle with rounded corners. The length, along which laser light is absorbed, was 1.2mm with a width of 2 mils. This results in a detector area about 7 times as large as those used to detect GaAs laser wavelengths. The epitaxial layer was 15μm thick with a doping level of $1\times10^{15}cm^{-3}$.

The experimental arrangement was similar to that shown in Fig. 10 for GaAs lasers, except that a Nd:YAG laser with

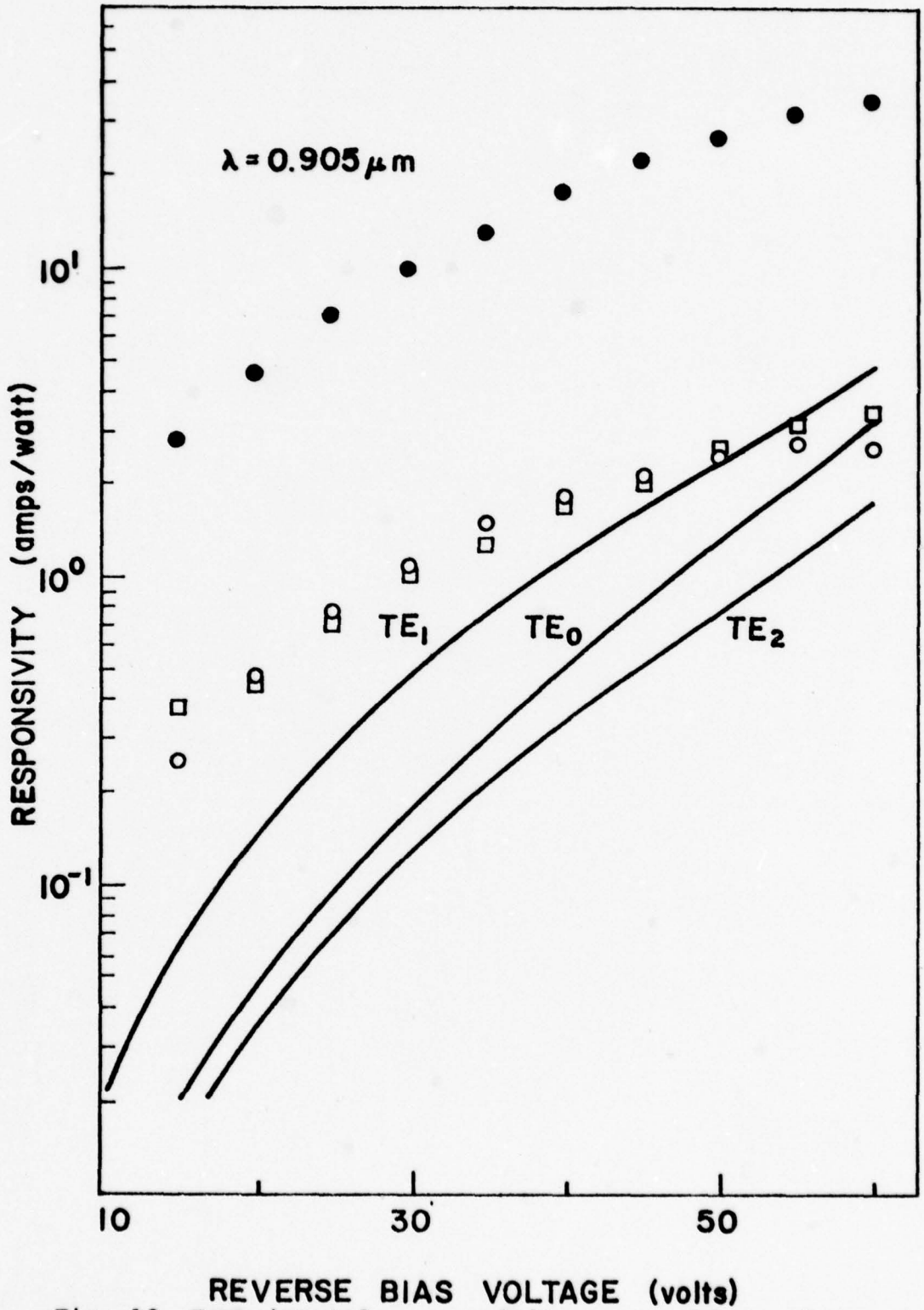

Fig. 13 Experimental responsivity versus bias voltage at 0.905μm.

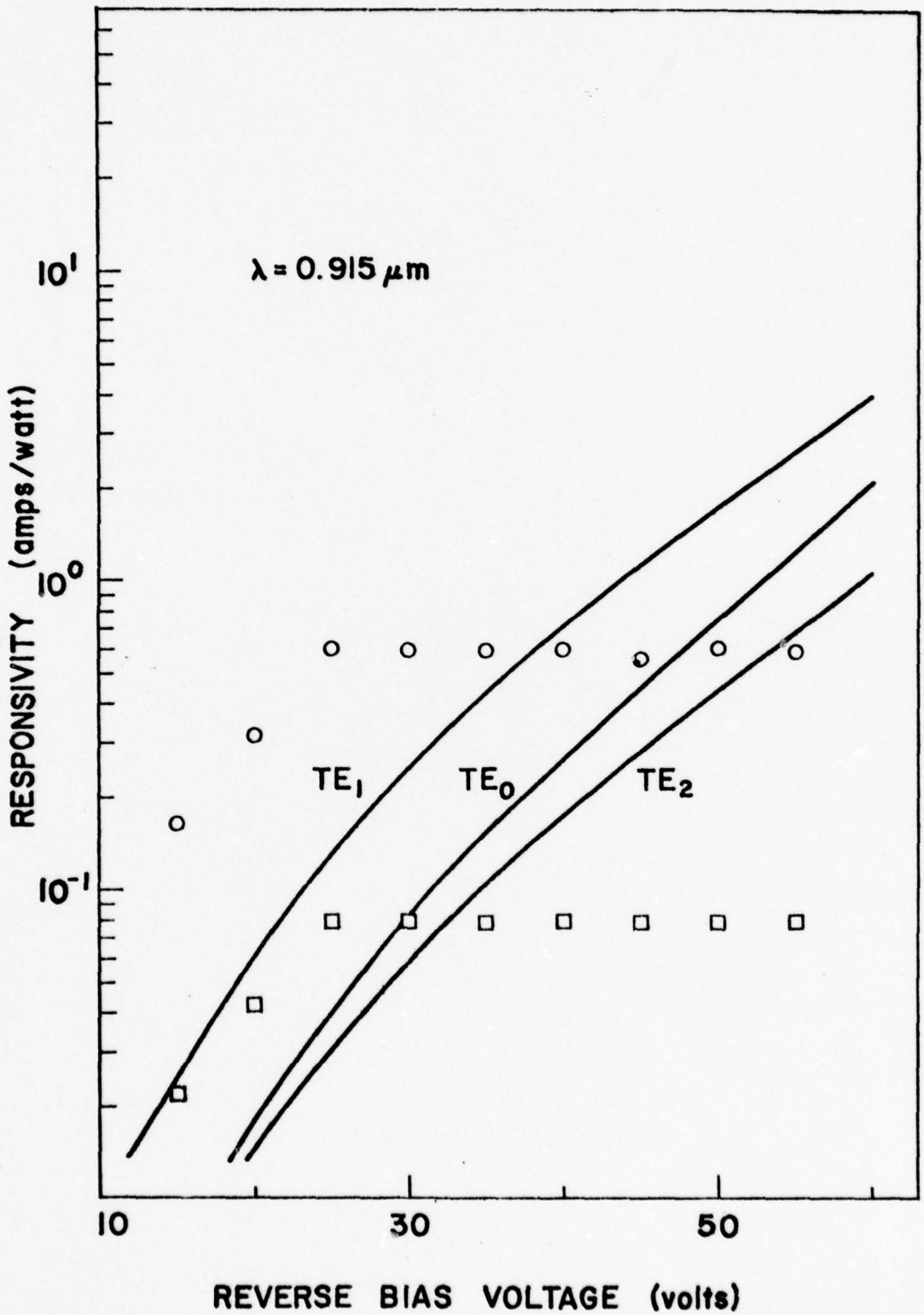

Fig. 14 Experimental responsivity versus bias voltage at 0.915μm.

appropriate filters to reduce the incident power on the waveguide detector was used. The absolute incident power to the EAP detector was determined by measuring the output power from the waveguide at zero detector bias with the light-mike and correcting for reflection. The reflection loss at 1.06μm is about 0.30 which resulted in an incident laser power of 7.1×10^{-6} watt. With this power at 1.06μm the EAP detector photocurrent was measured as a function of reverse bias voltage. The resulting responsivity is shown in Fig. 15. At the maximum responsivity the absorption coefficient was determined to be $1.6cm^{-1}$.

4.4 Response Speed

Since the electroabsorption process is electronic, it is expected to be very fast and should impose no limit on the response time which can be obtained with GaAs EAP detectors. The limiting factor to the response time of these detectors is expected to be due to transit time or RC effects. For the 4-mil diameter detectors in 10μm waveguides used to detect the GaAs laser emission, we estimate a transit time of 100psec and an RC time of 180psec . For the 1.2mm×2mil detectors in 15μm waveguides used to detect the Nd:YAG laser emission, we calculate a transit time of 150psec and an RC time of 900psec. Thus, the limitation for both geometries is expected to be the RC response. The transit-time estimates assume punch-through operation and saturated drift velocity, while the RC estimates are based on measured series resistance and geometry.

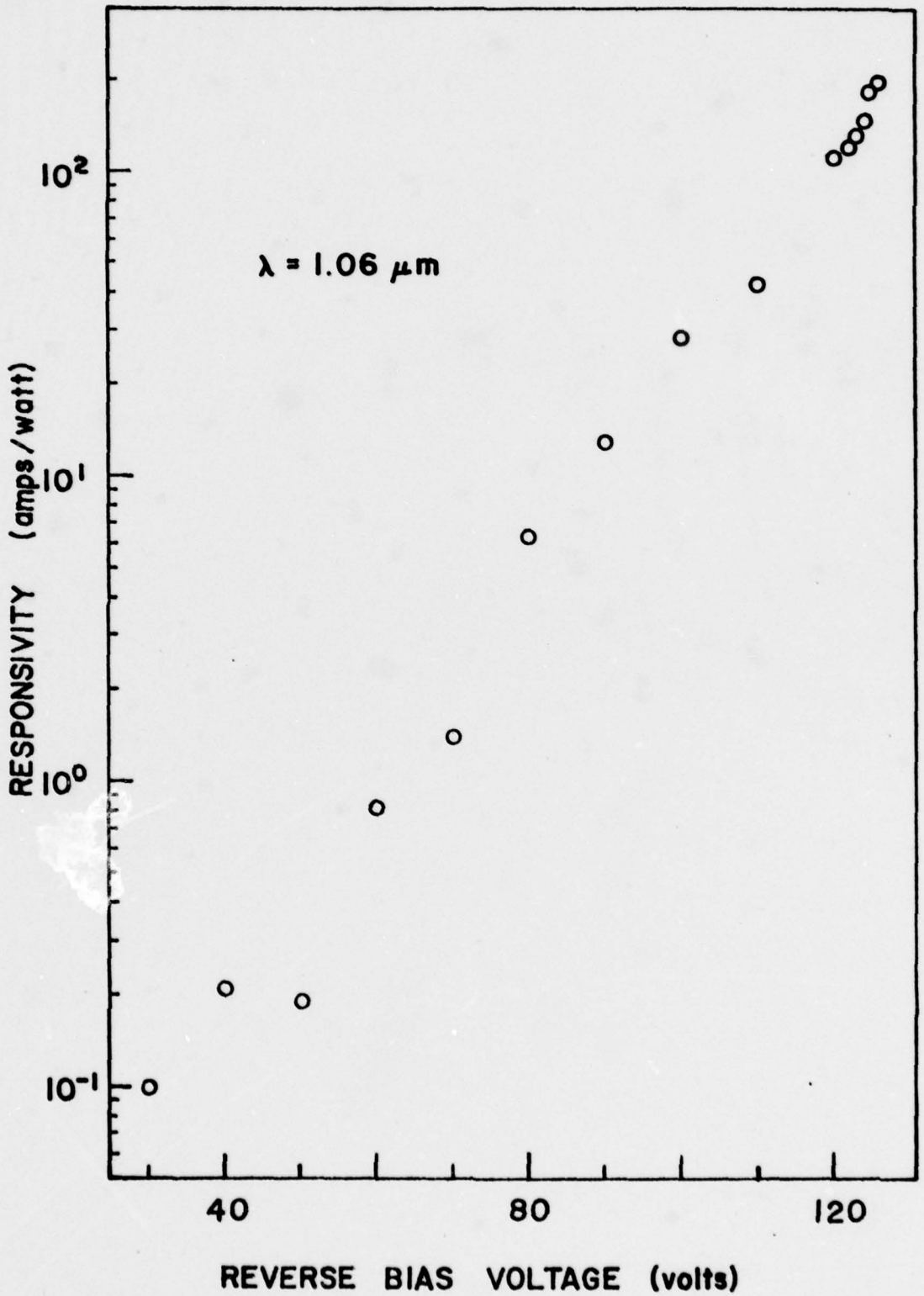

Fig. 15 Experimental responsivity versus bias voltage at 1.06μm.

Although we have not been able to test these estimates experimentally on waveguide EAP detectors, response time measurements have been performed[8] on discrete EAP detectors of comparable geometry. These measurements on discrete GaAs EAP devices indicated rise and fall times of less than 1nsec. This value, however, was close to the limitation imposed by the measuring apparatus.

5. APPLICATIONS

We now consider the applicability of GaAs EAP waveguide detectors for processing analogue or digital optical signals.

5.1 Analogue Detection

For applications involving the detection of analogue signals, it is desirable to know how faithfully the detector will convert optical information into electrical form. To determine this experimentally a laser diode DC-biased above threshold can be sine-wave modulated electrically, the modulated optical signal from the laser detected by the EAP device, and the modulated electrical signal from the detector analyzed for harmonic content. Since the optical output from the laser is a nonlinear function of the electrical input and the electrical output from the detector is a nonlinear function of the optical input, it is first necessary to examine the DC input-output characteristics of both the laser and the detector to determine a suitable operating point.

For this purpose a CW AlGaAs-GaAs mounted to a heat sink was connected to a regulated DC current source in series with a 4.7ohm resistor. The CW laser emission wavelength was 0.88μm, which is strongly attenuated by the GaAs waveguide.[9] For this reason it was necessary to operate the detector as a discrete device as opposed to a waveguide device. The output of the laser was collected by a lens and focused about 24cm from the lens. A light-mike was placed slightly ahead of the focal point to prevent damage to the detector. The light-mike was then aligned so that light absorption was maximized. The laser output power was then measured as the input current was varied. The resulting data are plotted in Fig. 16. As can be seen, this characteristic has a sizeable linear region in which the AC measurements can be performed.

The detector used was an aluminum Schottky barrier EAP device in a waveguide 12μm thick, with a carrier concentration of $3.6\times10^{15}cm^{-3}$ which was mounted on a header. The laser circuit was the same as that used for the laser power output measurements. The detector was connected to a DC voltage supply, and the photocurrent measured with an electrometer. The photocurrent of the detector versus the laser output power for a detector bias of 70 volts is given in Fig. 17. Figure 18 shows the circuit used for the AC measurements. The laser was DC biased at 250 milliamps to put the laser in the linear region of the input current versus output power characteristic shown in Fig. 16. To modulate the laser a 50 MHz power oscillator was used. The power

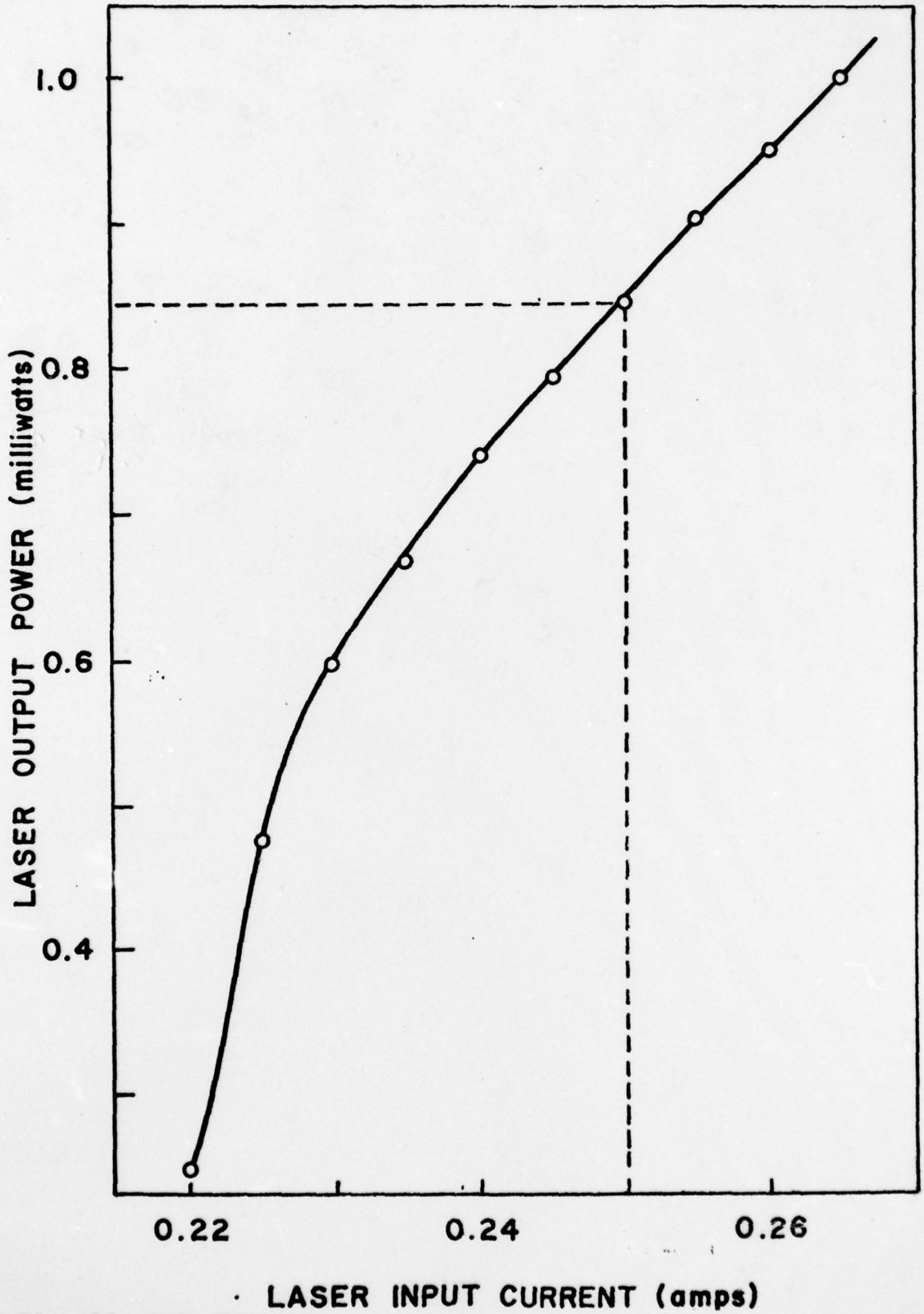

Fig. 16 GaAs CW laser input-output characteristic. The dashed line indicates the operating point for AC measurements.

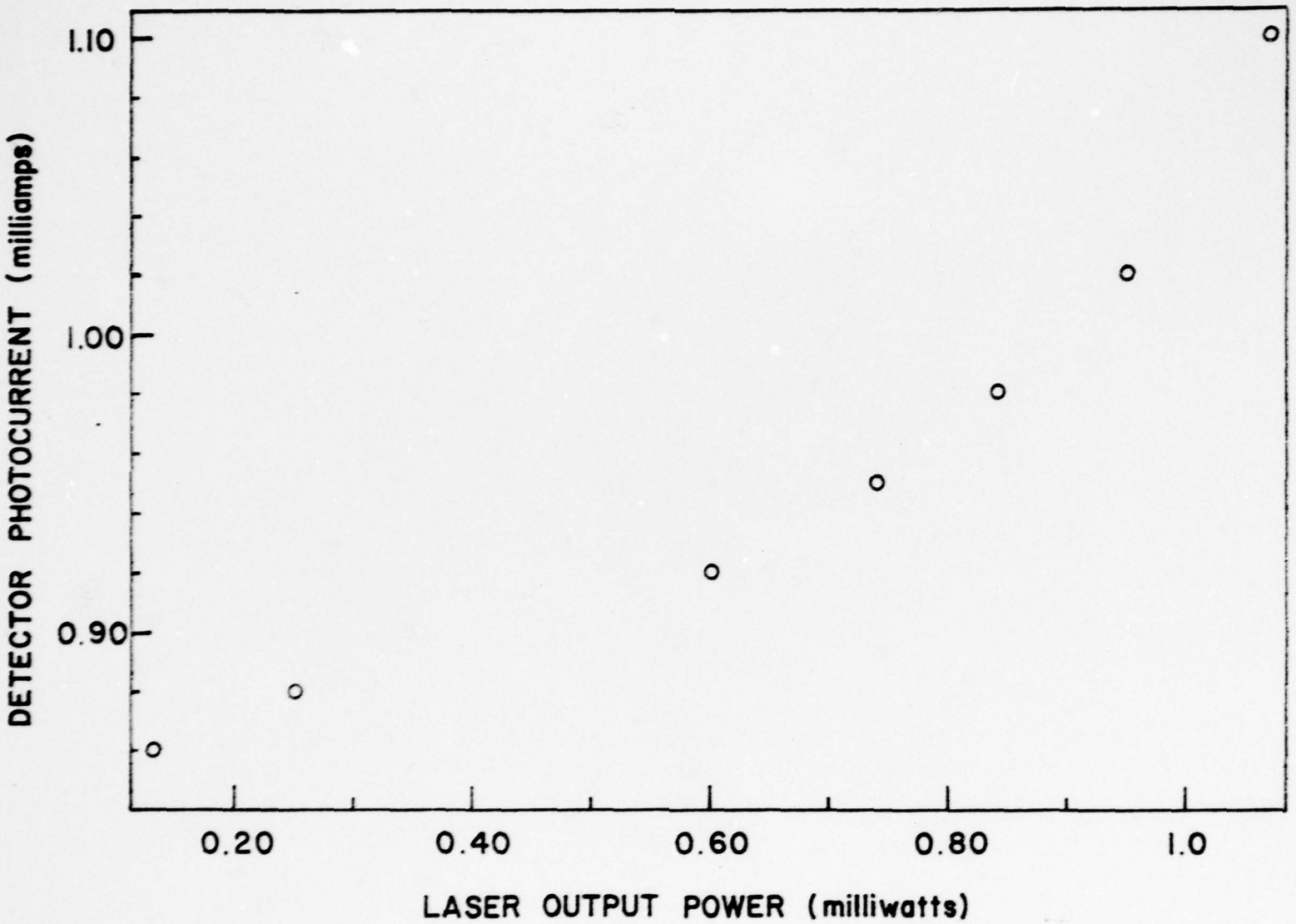

Fig. 17 GaAs EAP detector input-output characteristic.

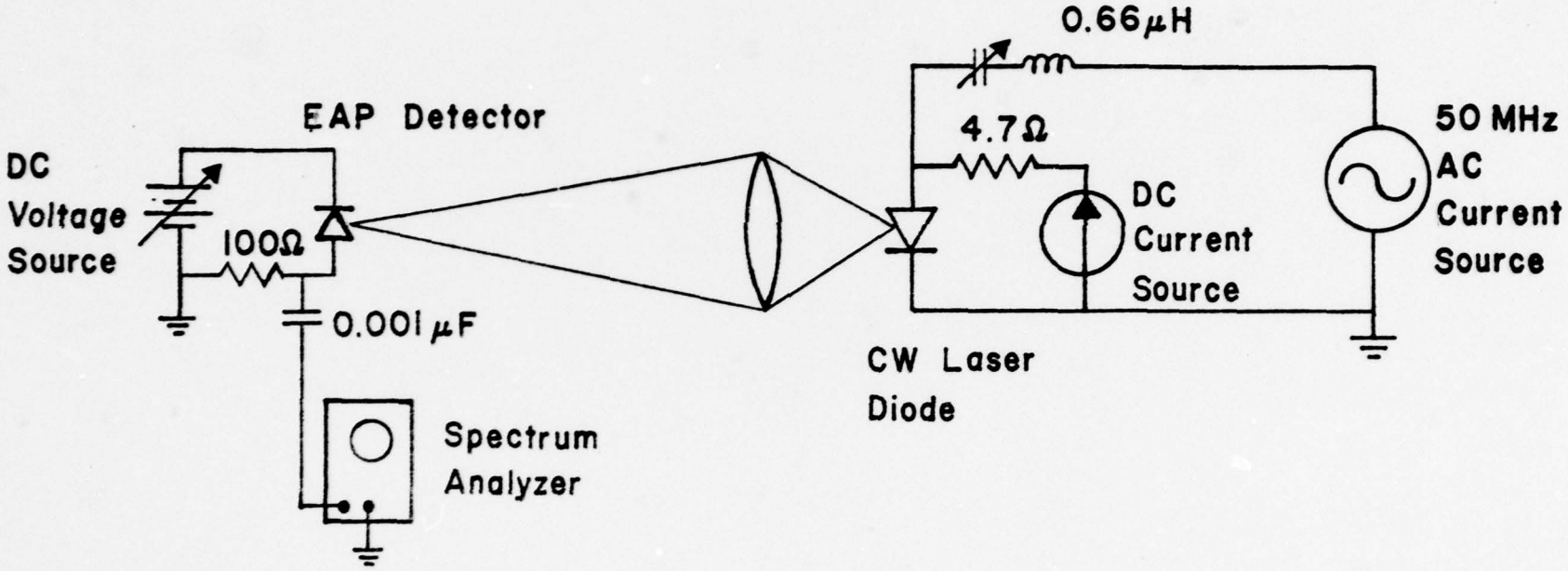

Fig. 18 Diagram of experiment used to measure the harmonic distortion of EAP detectors.

oscillator was isolated from the DC circuit with a variable capacitor. To help match the impedence of the laser to the 50MHz oscillator a 0.66μH inductor was added to the variable capacitor. This enabled the circuit to be tuned to maximize the power modulation. This tuning was performed with a light-mike to observe the laser output. At maximum power modulation the AC peak-to-peak power output was only 30% of the total DC power output. Thus, the AC output power swing of the laser remains in the linear region of the characteristic shown in Fig. 16, and most of the measured distortion should be due to the EAP detector.

The photocurrent of the detector was determined by measuring the voltage across a 100-ohm resistor. The DC was blocked with a 0.001μf capacitor in series with the spectrum analyzer. The detector was reverse-biased at 70 volts, and the AC photocurrent varied by changing the power modulation from 0 to 30%. The fundamental frequency was measured to be 57.5 MHz. The harmonics were then measured to give relative amplitude differences. It was found that the second harmonic was 12 to 16 db below the fundamental in power input. The third harmonic was 22 to 27db below the fundamental. The fourth harmonic was 22 to 29db below the fundamental, and the fifth harmonic could not be measured because of the scale limitations of the spectrum analyser. These values result in harmonic distortion of between 2.6 and 6.3% for the EAP detector as the peak-to-peak photocurrent output is varied from 20 to 80μamps.

5.2 Time Demultiplexing

Another application for the GaAs EAP waveguide detector is in a high-data-rate time-demultiplexing receiver. Because of its high-speed and low distortion the detector can easily reproduce digital information, and the main problem is the receiver's electronic circuitry. Synchronization between the transmitted signals and the receiver's counting circuit is the most important and most difficult part, especially for high-data-rate communication. The presently existing logic circuits have an upper limit of about 40Mbps pulse rate. To demonstrate a time demultiplexing scheme, a coded pulse train containing three channels with 12 bits in each channel was sent out from a laser or LED transmitter diode. A coding circuit was designed to drive a current amplifier which, in turn, was used to pulse the transmitter. A time demultiplexing circuit was then designed for the output of the photodetector. The signal detected by the photodiode had to be amplified to a voltage value above 1.5V, since it is the minimum value required to drive a logic circuit. The transmitter coding circuit and the time demultiplexing circuit are shown in Figs. 19 and 20, respectively. A noise clipper circuit is also included at the output of the time demultiplexing circuit. Figure 21(a) shows the three-channel multiplexed optical signal input to the detector. Figures 21(b), (c), and (d) show the three demultiplexed channels at the receiver end. The pulse rate for this experiment was 1Mbps. A pulse of wider width in front of the first channel was used as

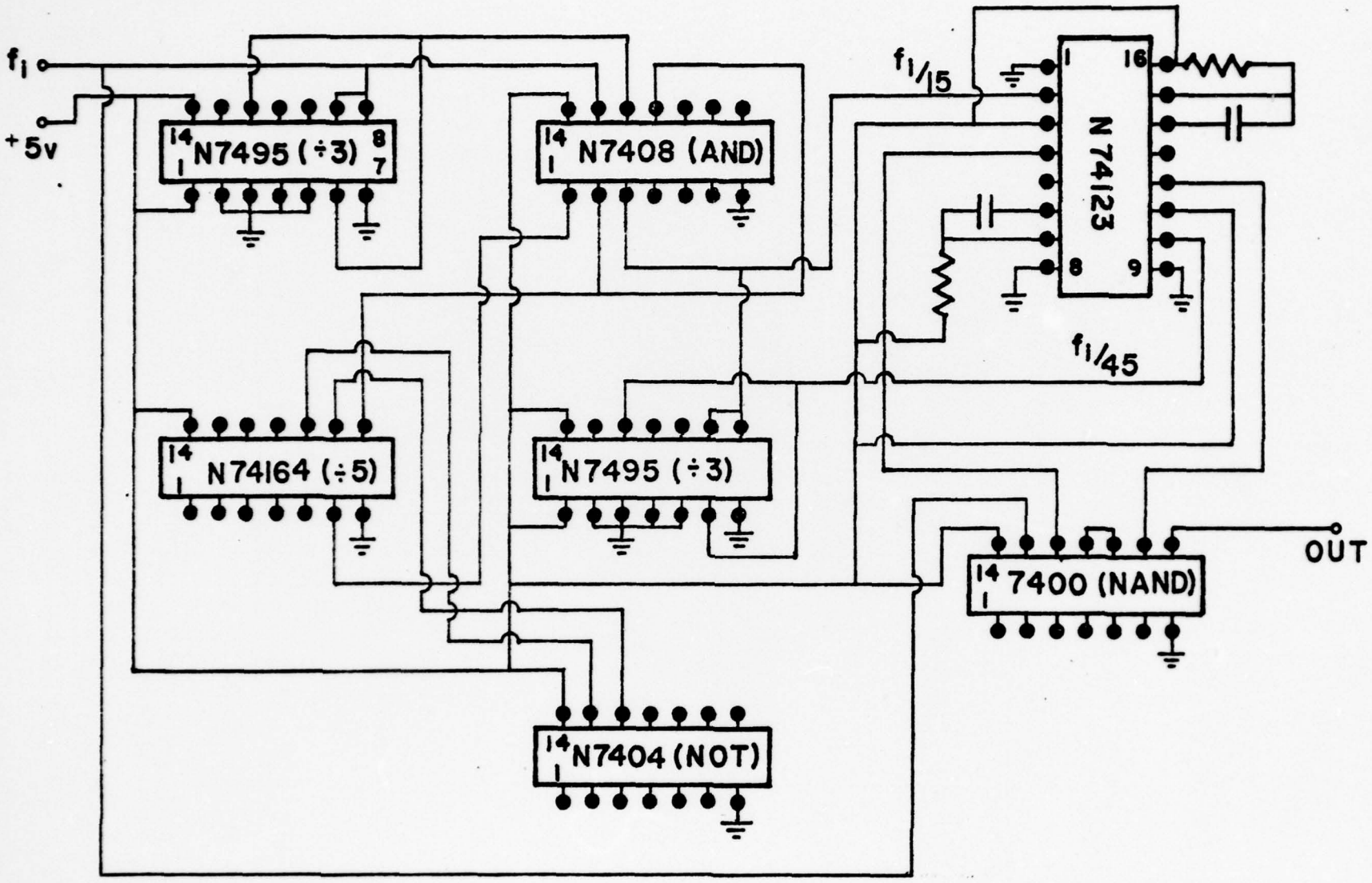

Fig. 19 Coding circuit for multiplexing GaAs laser transmitter.

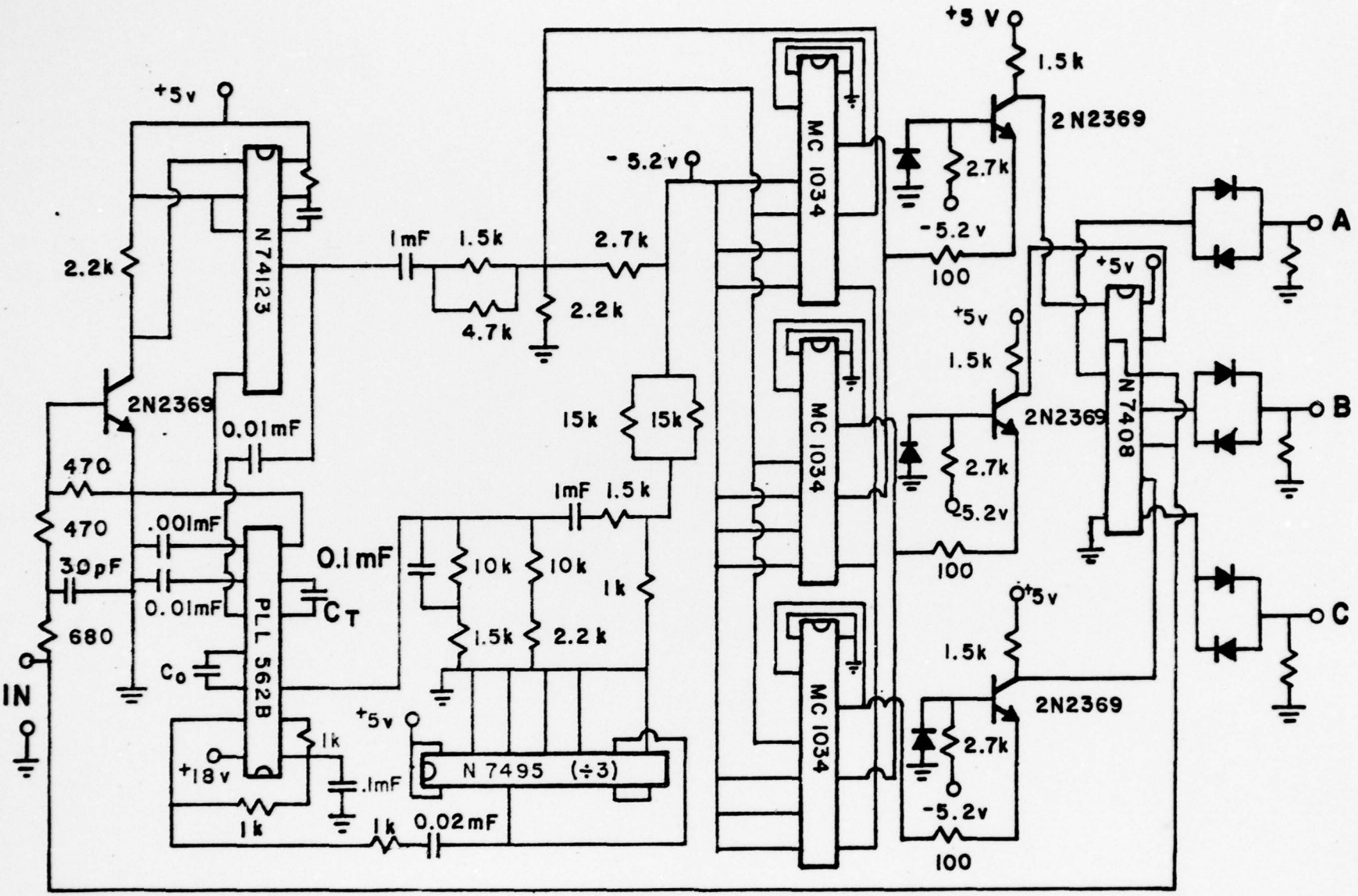

Fig. 20 Circuit for time demultiplexing receiver.

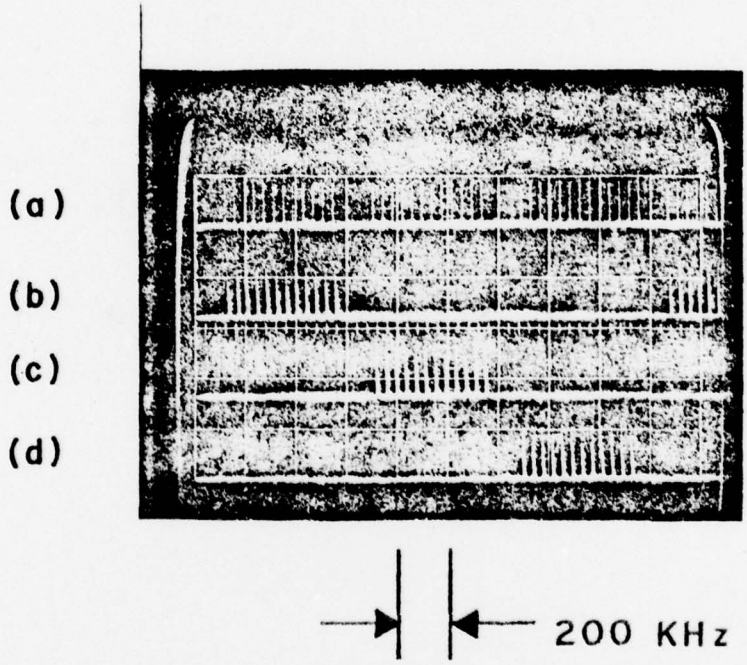

Fig. 21 Results of time-demultiplexing experiments

(a) is the 12-bit, 3-channel input.

(b), (c), and (d) show the 3 separated output channels.

a synchronizing pulse. If the propagation delay in the circuit is significant, then a delay line has to be inserted in the synchronizing circuit. Because a suitable laser of wavelength 0.905μm or longer with a duty factor larger than 1% was not available to demonstrate operation above 1Mbps, a LED was used as the transmitter in this experiment

In the time demultiplexing circuit shown in Fig. 20 the longer synchronizing pulses are picked up by the pulse width discriminator, which is essentially a RC filter plus a diode switch. The diode is so biased that its output swings between 0 and 5V. The synchronizing pulses are then fed into a monostable multivibrator to be reshaped. The reshaped pulses are then sent to the phase-locked loop, whose free running pulse rate is set to be equal to three times the rate of the input pulse. The signal pulses are locked to the phase-locked loop through a 3-to-1 frequency divider. The output of the phase-locked loop then has a pulse rate equal to the information rate, and is synchronized to the input information. The following circuits are timimg gates for each channel. Each channel then passes through a noise clipper to remove circuit noise. As previously indicated, the outputs are shown in Figs. 21(b), (c), and (d).

5.3 Frequency Demultiplexing

The final application we consider is one that is unique to the GaAs EAP waveguide detector. That is, by varying the bias on an EAP detector it can be used as a frequency-selective element. This is indicated in Fig. 3. Frequency demultiplexing can be achieved by passing a multi-frequency optical beam through a row of two or more EAP detectors. The bias voltages of the detectors are arranged in an increasing order so that the shortest wavelength signals are detected by the first diode (with the lowest bias voltage) and that the longest wavelength signals are detected by the last diode (with the highest bias voltage). In addition, device lengths can be altered to vary the absorption.

Although this frequency demultiplexing technique has the advantage of simplicity, the signals must be detected in order of increasing wavelength. In addition, the first detector will pick up some fraction of the longer wavelength signal intended for the second detector, etc. This constitutes the dominant mechanism for cross-talk among frequency channels.

The cross-talk among frequency channels can be estimated by using Eq. (2-14) for the equivalent absorption coefficient. Considering a three-channel GaAs laser multiplexing system with a wavelength separation of 0.03μm (which can be achieved with silicon-doped active regions[9]), EAP detector biases and lengths were varied to obtain a calculated minimum signal-to-noise ratio in the receiver channel of 10db. From this analysis the optimum detector configuration was: first detector biased at 0.15 of

the breakdown voltage with a length of 100μm; second detector biased at 0.35 of breakdown with a length of 300μm; and third detector biased at 0.9 of breakdown with a length of 300μm. This configuration gives calculated signal-to-noise ratios of 16, 10, and 11db for the first, second, and third detectors, respectively. Considering a two-channel system with the same wavelength separation, the signal-to-noise ratio can be made arbitrarily large. However, it is not possible to obtain a four-channel demultiplexing system with a minimum signal-to-noise ratio of 10db for each channel using EAP detectors.

Experimentally, because of the limited commercial availability of laser diodes of different wavelength, a two-channel system with a wavelength separation of 0.01μm was investigated. The results are shown in Figs. 11 and 12 and Fig. 13 and 14 for detectors with the same geometry. As can be seen, even with this small wavelength separation, for a two-channel system the cross-talk between channels can be made arbitrarily small by varying the detector bias.

6. CONCLUSIONS

GaAs EAP waveguide detectors show substantial promise for applications involving the processing of analogue or digital optical information from GaAs or Nd:YAG lasers. At GaAs laser wavelengths they can be fabricated on the same substrate as the GaAs laser with other components, and can be used to detect the below-energy-gap radiation of GaAs lasers transmitted through GaAs waveguides.

Experimentally, equivalent absorption coefficients as high as 130cm^{-1} with responsivities of 40amps/watt have been obtained at 0.905μm. This corresponds to a gain of about 70 for the EAP detector in waveguide configuration. At 1.06μm an absorption coefficient as high as 1.6cm^{-1} has been attained with a responsivity of 200 amps/watt. Analysis of the electroabsorption and avalanche processes indicate that this performance can be improved with improvements in the detector fabrication processes.

An analysis of the factors which limit the response speed of the GaAs EAP waveguide detectors indicates a limitation of about 100psec (depending upon geometry) for high-speed applications. Measurements of the harmonic content of the photocurrent output for these detectors with a 50MHz sinusoidal optical input indicate a distortion of between 2.6 and 6.3%. These values are sufficiently low for most analogue applications. For digital signals the EAP detectors can be used in time- and frequency-demultiplexing receivers. In a two-channel frequency-demultiplexing system the cross-talk between EAP detectors can be made arbitrarily small by varying bias. In a three-channel system a signal-to-noise ratio of 10db per channel can be obtained by varying bias and geometry.

REFERENCES

1. G.E. Stillman and C.M.Wolfe, "Avalanche Photodiodes" in *SEMICONDUCTORS AND SEMIMETALS, VOL. 12, INFRARED DETECTORS*, Eds. R.K. Willardson and A.C. Beer, (Academic Press, New York, 1977).

2. W.T. Lindley, R.J. Phelan, Jr., C.M. Wolfe, and A.G. Foyt, *APPL. PHYS. LETTERS*, 14, 197 (1969).

3. G.E. Stillman, C.M. Wolfe, J.A. Rossi, and J.P. Donnelly, *APPL. PHYS. LETTERS*, 25, 671 (1974).

4. G.E. Stillman, C.M. Wolfe, J.A. Rossi, and J.L. Ryan, *PROC. 5TH INT. SYMP. GaAs*, (Inst. Phys., London, 1975), 210.

5. W. Franz, *Z. NATURFORSCH*, A13, 494 (1958); L.V. Keldysh, *SOV. PHYS.-JETP*, 34, 788 (1958).

6. C.M. Wolfe, G.E. Stillman, and J.O. Dimmock, *J. APPL. PHYS.*, 41, 504 (1970).

7. C.M. Wolfe and W.T. Lindley, *J. ELECTROCHEM. SOC.*, 116, 276 (1969).

8. G.E. Stillman, C.M. Wolfe, J.A. Rossi, and J.L. Ryan, *PROC. INT. SYMP. OPT. ACOUST. MICROELECTRONICS*, (Polytechnic Inst. N. Y., New York, 1974), 543.

9. G.E. Stillman, C.M. Wolfe, J.A. Rossi, and H. Heckscher, *APPL. PHYS. LETTERS*, 28, 197 (1976).